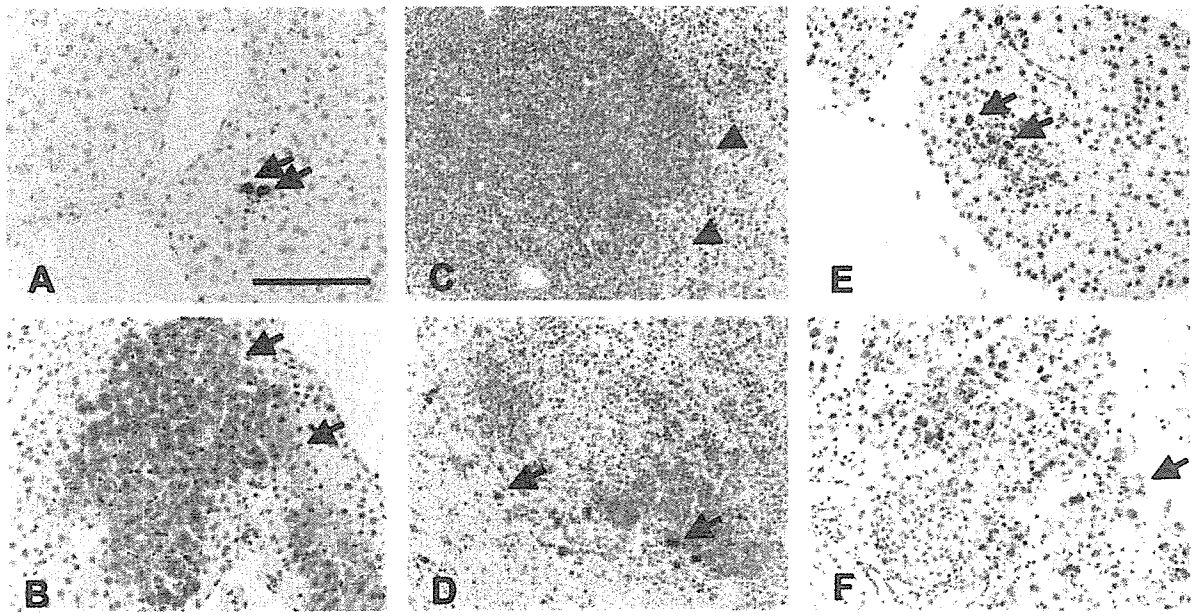

FIG. 2. Immunohistochemical detection of poliovirus antigen in infected mice. Poliovirus antigens were detected in PVR-transgenic (A, C, and E) and PVR-transgenic/*Ifnar* knockout (B, D, and E) mice with a rabbit polyclonal antibody recognizing the poliovirus capsid antigen. The mice were intravenously inoculated with 2×10^7 PFU of poliovirus. (A) Liver of the PVR-transgenic mice on day 1 p.i. Poliovirus antigen-positive cells, indicated by arrows, were focally observed with slight cellular infiltration around the infected cell. (B) Liver of PVR-transgenic/*Ifnar* knockout mice on day 1 p.i. Hepatic cells positive for poliovirus were observed in a zonal pattern. (C) Spleen of PVR-transgenic mice on day 1 p.i. A few very weakly stained cells are observed in the marginal zone, indicated by arrowheads. (D) Spleen of PVR-transgenic/*Ifnar* knockout mice on day 1 p.i. Many poliovirus antigen-positive large cells are localized in the marginal zone. The cells were identified as macrophages on the basis of the detection of CD11. (E) Pancreas of PVR-transgenic mice on day 3 p.i. A small cluster of cells positive for poliovirus antigen was observed in the lobulus in association with a slight inflammatory reaction. The poliovirus antigen was observed constantly in all mice. (F) Pancreas of PVR-transgenic/*Ifnar* knockout mice on day 3 p.i. Numerous acinar cells positive for the poliovirus antigen were distributed in many lobuli of the pancreas. Only a few poliovirus antigen-positive cells were observed in Langerhans' islets in the bottom left. (A) Bar, 125 μm.

tion of the poliovirus antigen and corresponding pathological changes to determine the virus replication sites. In the liver of PVR-transgenic mice, cells positive for the poliovirus antigen were detected occasionally, after careful observation. The antigens were found sporadically as a single cell or as a group of a few poliovirus antigen-positive cells with cellular damage in the liver on day 1 p.i., but were rarely detected after day 2 p.i. Inflammatory cell infiltration was also observed around the infected cells (Fig. 2A). Strong poliovirus antigen staining was not detected in the spleen, but a few very weakly stained cells were observed in the marginal zone (Fig. 2C). In the pancreas, groups of a few poliovirus antigen-positive cells were sporadically observed on day 1 p.i., with the number increasing slightly on day 3 p.i. (Fig. 2E). Although the infected area in the pancreas was not large, the antigens were always detected in all the mice. This observation is consistent with a higher poliovirus titer in the pancreas than in the other visceral tissues (Fig. 1).

In contrast, in PVR-transgenic/*Ifnar* knockout mice, zonal areas or clusters of poliovirus antigen-positive cells were observed in the liver on day 1 p.i. (Fig. 2B). These infected cells were identified morphologically as hepatocytes. The number of poliovirus antigen-positive cells decreased on day 3 p.i., but the inflammatory infiltrate became more evident. In the spleen, poliovirus antigen was detected mainly in large mononuclear cells in the marginal zone (Fig. 2D). These large mononuclear cells were positive for CD11 in serial sections and were shown to be macrophages (data not shown). In the pancreas, massive infection was observed in acinar cells (Fig. 2F).

The destruction of hepatocytes and pancreatic acinar cells was also confirmed by biochemical examination. Serum ALT and amylase levels were measured in intravenously inoculated mice on day 3 p.i. ALT values increased markedly in the PVR-transgenic/*Ifnar* knockout mice compared to the nontransgenic mice ($P < 0.05$, t test), whereas there was only a slight increase in the PVR-transgenic mice (Fig. 3A). This result indicates destruction

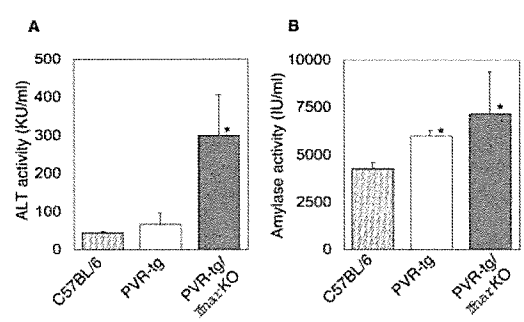

FIG. 3. Serum ALT and amylase activities in infected mice. The mice were inoculated intravenously with 2×10^7 PFU of poliovirus. The sera of nontransgenic (hatched bars), PVR-transgenic (open bars), and PVR-transgenic/*Ifnar* knockout (solid bars) mice were collected on day 3 p.i., and their ALT activity (A) and amylase activity (B) were determined. The mean values plus standard deviation of four mice are shown. The asterisks indicate that the values are significantly higher than those observed in the nontransgenic C57BL/6 mice ($P < 0.05$, t test).

of hepatocytes in the PVR-transgenic/*Ifnar* knockout mice. The amylase activity values in the serum of PVR-transgenic mice were 1.3- to 1.5-fold (mean, 1.4-fold) higher than that of the nontransgenic mice ($P < 0.05$, t test), while those of PVR-transgenic/*Ifnar* knockout mice were 1.2- to 2.3-fold higher (mean, 1.7-fold) than that of nontransgenic mice ($P < 0.05$, t test) (Fig. 3B). The results indicated acinar cell destruction in the pancreas and/or salivary glands in PVR-transgenic and PVR-transgenic/*Ifnar* knockout mice. These observations further indicate that the loss of alpha/beta IFN signaling apparently alters the tissue tropism. The hepatocytes, acinar cells, and macrophages in the spleen became potentially permissive for poliovirus infection, indicating that they express host factors required to support poliovirus replication.

With PVR-transgenic/*Ifnar* knockout mice, the virus antigens were not clearly detected in the kidneys, heart, and lungs of poliovirus-inoculated mice. Similar experiments were performed with another PVR-transgenic mouse strain, PVRtg25 (46). In this mouse strain, *PVR* mRNA expression levels are higher than those of PVRtg21. We further crossed this strain with *Ifnar* knockout mice and examined the susceptibility of PVRtg25/*Ifnar* knockout mice to poliovirus. All of the inoculated mice became moribund with jaundice on day 1 p.i. Immunohistological examination revealed that viral antigen-positive cells were detected in the liver, spleen, pancreas, kidneys, and heart (data not shown). Poliovirus infection in the liver was associated with massive necrosis of the parenchymal cells, which was correlated with liver failure. This confirmed that poliovirus can also replicate in the kidneys and heart when IFN signaling is disrupted.

Role of IFN in poliovirus spreading in the body. The above data indicate that the IFN response is particularly effective in restricting virus replication in the visceral tissues. Viremia occurred as a consequence of virus multiplication in extraneural sites. It is possible that the IFN response influences virus titer and, accordingly, that IFN also contributes in decreasing the incidence of paralytic and fatal poliovirus infection by lowering the chance of poliovirus entry into the central nervous system. To demonstrate this, we compared the virus titers in PVR-transgenic and PVR-transgenic/*Ifnar* knockout mice. We determined virus titers in the plasma of PVR-transgenic and PVR-transgenic/*Ifnar* knockout mice infected intraperitoneally with poliovirus (10^3 PFU). This dose was employed because it is below the LD_{50} of the PVR-transgenic and above that of the PVR-transgenic/*Ifnar* knockout mice (see Table 1).

Expectedly, a very high titer (10^8 to 10^9 PFU/ml) of poliovirus was detected on day 3 p.i. in the PVR-transgenic/*Ifnar* knockout mice, resulting in the death of the mice at day 4 p.i. In contrast, less than 10^3 PFU of poliovirus/ml was detected in the PVR-transgenic mice between days 2 and 5 p.i., and it was no longer detected at day 7 p.i. (Fig. 4). These results suggest that some cells, if not all, that express PVR can act as reservoirs of poliovirus during the progression of the disease in the viremic phase. However, only a small proportion of these cells produce poliovirus with a low efficiency because of the inhibitory effect of IFN, and high-titer viremia is prevented in animals with a normal IFN system. We consider that virus replication sites during the viremic phase have not been histologically identified because poliovirus replication levels are normally low in these cells in PVR-transgenic mice, monkeys, and humans.

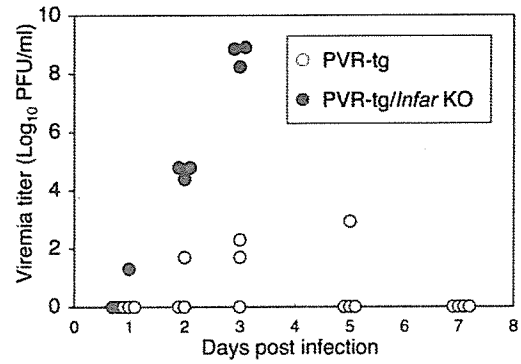

FIG. 4. Viremia in PVR-transgenic mice and PVR-transgenic/*Ifnar* knockout mice. Poliovirus (10^3 PFU) was inoculated intraperitoneally. Plasma from three or four infected mice was collected at the indicated day p.i., after which the virus titer in the plasma was determined. Open circles, PVR-transgenic mice; solid circles, PVR-transgenic/*Ifnar* knockout mice. Note that the virus titer in the PVR-transgenic/*Ifnar* knockout mice is very high. The data for PVR-transgenic/*Ifnar* knockout mice on days 5 and 7 p.i. were not available because all mice died on the fourth day after inoculation.

Expression of IFN-β and ISGs in the host. The susceptibility to poliovirus varied among the tissues. We therefore determined if the expression profiles of genes that confer an antiviral state in the IFN response were different between target and nontarget tissues. We determined the expression of mRNAs for IFN-β and ISGs with a quantitative real-time reverse transcription-PCR technique (Fig. 5). Since IFN-β is the first alpha/beta IFN induced after virus infection (36, 39, 41) and picornaviruses are known to be sensitive to OAS (7, 8) and protein kinase R (25), we focused on expression of IFN-β, OAS, and protein kinase R mRNAs. Of the ten genes that are similar to human OAS in the mouse genome, OAS1a, OAS1g, OAS2, OAS3, and OASL2 were shown to synthesize 2′-5′oligoadenylate (16).

We first determined the expression levels of IFN-β, OAS, and protein kinase R mRNAs in the noninfected PVR-transgenic mice. Very little expression of IFN-β mRNA was observed in all tissues of the noninfected mice (Fig. 5A). The expression levels of the mRNAs for OAS1a, OAS1g, OAS2, OAS3, OASL2, and protein kinase R are shown in Fig. 5B to G (open bars). The expression level of each ISG mRNA and the tissue distribution profiles were different. However, in general, they were expressed in the nontarget tissues more abundantly than in the target tissues of noninfected PVR-transgenic mice. No ISG was expressed at high levels in the central nervous system, an observation consistent with previous reports (1, 22, 30).

We then determined the changes in the expression levels of IFN-β and ISG mRNAs in the infected mice (Fig. 5A to G). On day 1 p.i., IFN-β mRNA expression in the spleen was observed at very high levels. Low-level IFN-β expression was observed in the heart, lungs, liver, kidneys, and muscle. No significant increase of IFN-β mRNA was observed in the brain and spinal cord on day 1 p.i. (Fig. 5A, gray solid bars). On day 3 p.i., IFN-β mRNA levels in the heart, lungs, liver, kidneys, and muscle decreased to nearly basal levels. In contrast, they increased to very high levels in the brain and spinal cord (Fig. 5A, solid black bars). Thus, the IFN-β mRNA expression pro-

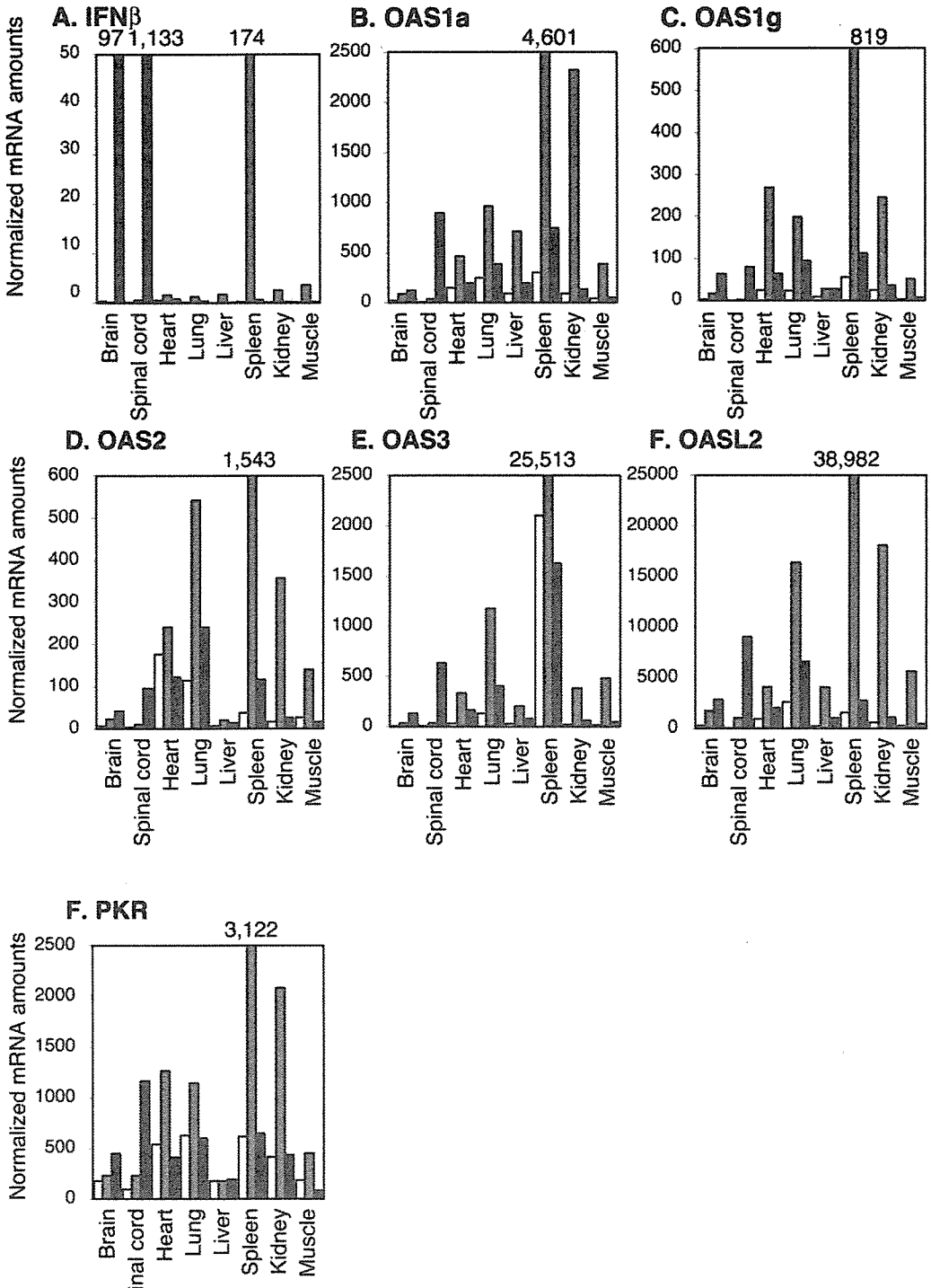

FIG. 5. Expression of IFN-β and ISGs in PVR-transgenic mice. The expression levels of IFN-β and ISG mRNAs in noninfected PVR-transgenic mice and PVR-transgenic mice infected intravenously with poliovirus (2×10^7 PFU) were determined by real-time quantitative PCR. The amounts of IFN-β (A), OAS1a (B), OAS1g (C), OAS2 (D), OAS3 (E), OASL2 (F), and protein kinase R (G) mRNAs normalized to 10^7 copies of 18S rRNA are shown. Open bars, gray solid bars, and black solid bars indicate the results for noninfected mice, infected mice at 1 day p.i., and infected mice at 3 days p.i., respectively. The mean values for three to six mice are indicated. The numbers above each figure indicate values that could not be represented within the figures. Note that the open bars in A are not visible because IFN-β mRNA expression in the noninfected mice was very low.

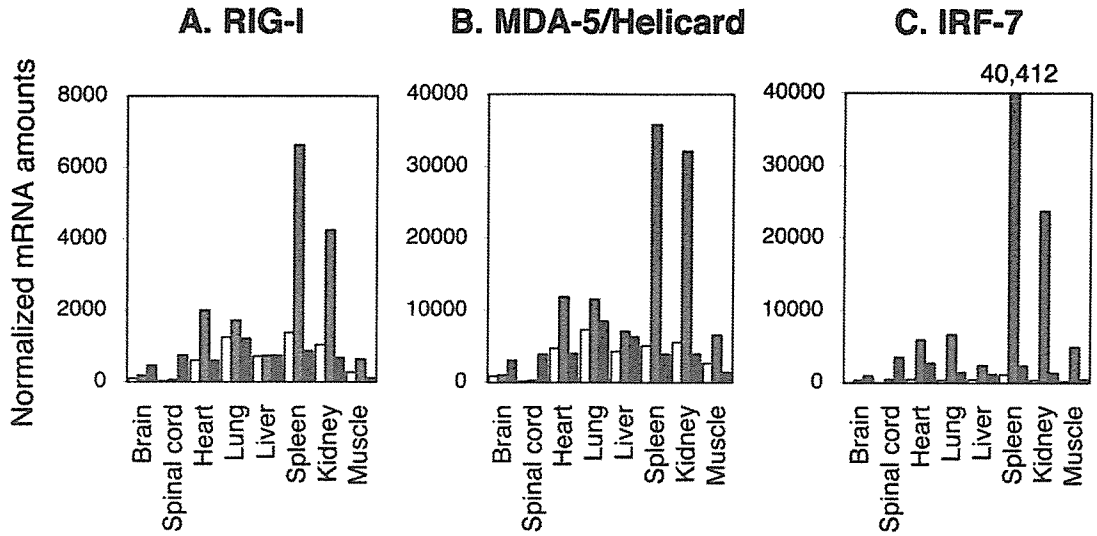

FIG. 6. Expression of RIG-I, helicard, and IRF-7 mRNAs in PVR-transgenic mice. The expression levels of RIG-I, helicard, and IRF-7 mRNAs of noninfected PVR-transgenic mice and PVR-transgenic mice infected intravenously with poliovirus (2×10^7 PFU) were determined by real-time quantitative PCR. The mean values for three mice are indicated. The amounts of RIG-I (A), helicard (B), and IRF-7 (C) mRNAs were determined. Open bars, gray solid bars, and black solid bars indicate the results of noninfected mice, infected mice at 1 day p.i., and infected mice at 3 days p.i., respectively. The amounts of mRNA per 10^7 copies of 18S rRNA are shown.

files are different between target tissues and nontarget tissues in poliovirus-infected mice.

The expression levels of ISG mRNAs also changed after poliovirus infection, consistent with the change in IFN-β mRNA levels (Fig. 5B to G, gray and solid black bars). The ISG expression pattern was clearly different between the target and nontarget tissues. ISG mRNAs increased in most of the visceral tissues on day 1 p.i. The expression level of ISG mRNAs increased most efficiently in the spleen. The levels of ISG mRNAs were relatively high in the heart, lungs, liver, kidneys, and skeletal muscle. In these tissues, the viral load was low (Fig. 1), and the poliovirus antigen was not detected. This indicates that ISG induction in these tissues was sufficient to inhibit poliovirus replication. The expression levels of ISG mRNAs in these tissues decreased on day 3 p.i., with a corresponding decrease in IFN-β mRNA levels. In the brain and spinal cord, however, significant induction of ISG mRNAs was not observed on day 1 p.i. The induction became evident only on day 3 p.i., when poliovirus destroyed a large number of neurons. We also noticed that the ratio of ISG and IFN-β mRNAs (ISG/IFN-β mRNA) in the brain and spinal cord on day 3 p.i. was much lower than that in nontarget tissues on day 1 p.i. (Fig. 5A to G). This indicates that the IFN response did occur in neurons in the brain and spinal cord but was not sufficient and failed to inhibit viral growth in the early phase of infection.

Expression of RIG-I, MDA-5/helicard, and IRF-7 in target and nontarget tissues. The data suggests that neurons in the target tissues failed to respond sufficiently to poliovirus infection. It is possible that there is a difference in the expression mechanism of the IFN response. We proceeded to examine a regulatory factor required for IFN response. Yoneyama et al. recently found that RIG-I functioned as a detector of intracellular double-stranded RNA. The cells that express this gene at high levels in vitro can induce IFN in an accelerated fashion and can survive against encephalomyocarditis virus and vesicular stomatitis virus infection (48). MDA-5/helicard is another caspase recruitment domain (CARD)-containing helicase, which is implicated as having a function similar to that of RIG-I (48). Both RIG-I and MDA-5/helicard are inducible by IFNs (17, 48).

Figures 6A and B show the changes in the RIG-I and MDA-5/helicard levels, respectively. Like that of other ISGs, the expression of these genes is low in the brain and spinal cord but high in nontarget tissues in the noninfected mice. The response of these genes after poliovirus infection is similar to that of other ISGs. They were induced at high levels in the nontarget tissues on day 1 p.i. but not in the target tissues. Thus, the nontarget tissues that expressed RIG-I and MDA-5/helicard at high levels may have an advantage in inducing IFN-β soon after poliovirus infection. We also examined the expression of IRF-7, another regulatory factor involved in the activation of IFN-α genes. IRF-7 thus is important to amplify the IFN response (37). The expression profile of IRF-7 was also similar to those of other ISGs (Fig. 6C).

Protection of mice from poliovirus infection by poly(I:C) treatment. The preceding data suggest that neurons in the brain and spinal cord were highly susceptible to poliovirus because expression levels of ISGs, including OASs and RIG-I, were low in the noninfected state. If this is the case, pretreatment to induce the antiviral state in the central nervous system would increase the survival rate of poliovirus-infected mice. Hence, treatment with poly(I:C) is expected to induce IFNs and ISGs and establish an antiviral state.

Poly(I:C) (200 μg) was administered intracerebrally to PVR-transgenic mice, and on the next day, RNA was prepared from the brain and spinal cord. The levels of OAS1a and RIG-I were determined by real-time quantitative PCR. As expected, expression of the mRNAs for OAS1a and RIG-I was elevated to high levels by poly(I:C) (Fig. 7A and B). PVR-transgenic mice treated with poly(I:C) or mock treated were challenged with poliovirus

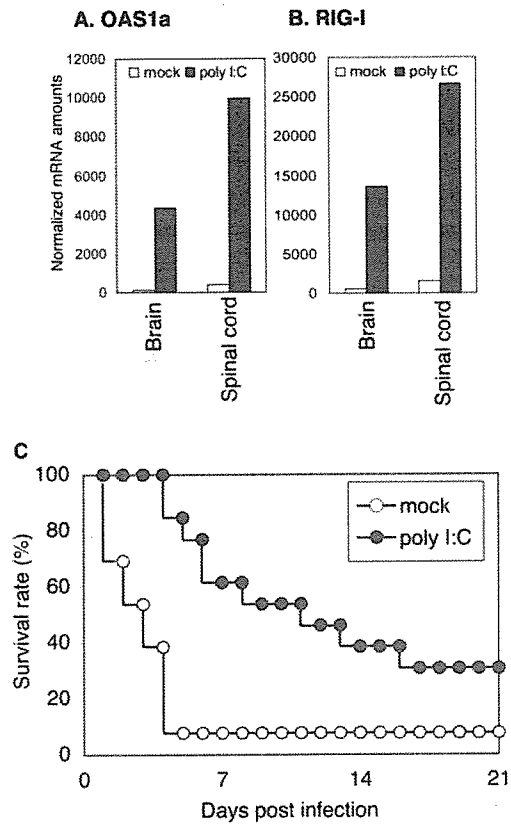

FIG. 7. Induction of mRNAs for OAS1a (A) and RIG-I (B) after poly(I:C) treatment. PVR-transgenic mice was administered poly(I:C) (solid bars) or mock treated (open bars). RNA was prepared from the mice 1 day after administration. The amounts of RNA were determined by real-time quantitative PCR. (C) Survival of infected mice. PVR-transgenic mice administered poly(I:C) (solid circles) or mock treated (open circles) (13 mice each) were challenged intracerebrally with 10^4 PFU of poliovirus. Mice were observed for 3 weeks. The survival rate of poly(I:C)-treated mice was significantly higher than that of mock-treated mice ($P < 0.05$, log-rank test).

(10^4 PFU) by the same route. The survival of the mice is shown in Fig. 7C. Mock-treated PVR-transgenic mice died at 2 to 6 days p.i., with a survival rate of 7.7%. After poly(I:C) treatment, mice died at 4 to 16 days p.i., increasing the survival rate to 30.8%. The clinical symptoms observed in the poly(I:C)-treated PVR-transgenic mice were almost the same as those observed in mock-treated mice, suggesting the same pathology. The results indicate that the poly(I:C)-treated mice survived longer than mock-treated mice, with the survival rate of poly(I:C)-treated mice being higher than that of mock-treated mice ($P < 0.05$, log rank test). These data suggest that the antiviral state induced by treatment with poly(I:C) was effective in preventing poliovirus replication in the central nervous system.

DISCUSSION

IFN system is a host factor that inhibits poliovirus replication. Picornaviruses are sensitive to IFNs. However, little is known about the role of alpha/beta IFN in the pathogenesis of poliovirus in vivo. We have shown the importance of the IFN response in poliovirus infection in vivo with a transgenic mouse expressing human PVR. In the PVR-transgenic mice, poliovirus replicates and produces severe lesions in the brain and spinal cord, while other tissues did not show severe pathological changes.

It would be reasonable to assume that some host factors required for poliovirus replication are lacking in the nontarget cells and tissues. PVR was thought to be such a determinant (13). However, previous studies revealed that many nontarget tissues expressed PVR (18, 21, 24, 31, 32). It is therefore impossible to explain poliovirus tissue tropism solely by the presence of PVR. Gromeier et al. (11) and Yanagiya et al. (46) proposed a hypothetical mechanism called the internal ribosome entry site (IRES)-dependent mechanism to explain the tissue tropism of viruses. The IRES controls the efficiency of protein synthesis in some viruses. Chimeric viruses containing the IRES of human rhinovirus and hepatitis C virus instead of the poliovirus IRES do not replicate in the central nervous system. Therefore, the poliovirus IRES confers the ability to replicate in neurons on the chimeric virus, while the IRESs of human rhinovirus and hepatitis C virus do not. It is possible that the poliovirus IRES, particularly in virulent strains, is designed to exhibit full activity in neurons. In this hypothesis, host factors related to poliovirus IRES function should be restricted to neurons. However, poliovirus can replicate in cultured cells of nonneural origin. This hypothesis does not completely explain why poliovirus does not replicate efficiently in nontarget tissues in vivo.

It is also possible to assume that some host factors that inhibit poliovirus replication are present in the nontarget tissues. The liver, spleen, and pancreas were spared severe poliovirus infection only when the IFN system was functional. These data demonstrate that the IFN system is one of the major factors that confers resistance against poliovirus infection. Limitation of poliovirus tissue tropism is achieved by inhibition of poliovirus replication by the IFN system in nontarget tissues. An altered tissue distribution of viral replication was observed in mice deficient in the *Ifnar* gene or in mice deficient in the signal transducer and activator of transcription 1 (*Stat-1*) gene infected with viruses other than poliovirus (9, 10, 28, 34, 44). In these animals, virus replication was observed in tissues that were normally considered nontarget tissues. Therefore, it is a general principle that the tissue tropism of viruses is determined, at least in part, by an IFN-dependent mechanism.

Unequal IFN response selectively inhibits poliovirus replication in nontarget tissues. In cultured cells, encephalomyocarditis virus replication occurs rapidly within 6 h, and the infected cells are usually destroyed by lytic replication of virus before they produce IFNs. However, constitutive expression of OAS or protein kinase R (7, 8, 25), which are effectors of antiviral activity, and expression of RIG-I (48), a regulator of IFN induction, inhibited viral replication. It is very likely that the same mechanism operates during poliovirus infection.

We determined the expression of ISGs in the tissues. The distribution of ISG mRNAs in the noninfected mice was not equal among tissues. They were expressed in the nontarget tissues more abundantly than in the target tissues (Fig. 5). These existing ISG products may help restrict virus replication and spread in the nontarget tissues during the initiation of infection in vivo. In PVR-transgenic/*Ifnar* knockout mice, the

expression levels of mRNAs for ISGs were greatly reduced. The mRNAs for OASs were detected only in the intestine and thymus (data not shown). This is also consistent with the result of Ueda et al. (43), which showed that OAS expression in most tissues was reduced in p48 (IRF-9)-deficient mice. This result suggests that ISG expression in most of the tissues, even in the noninfected state, is mainly dependent on the IFNAR-dependent pathway. It also suggests that these tissues were continuously exposed to IFN stimulation at low levels (43). Visceral tissues such as the intestine and lungs are continuously at risk of exposure to pathogens. These tissues may be programmed to respond readily to viral infection. Alternatively, they are constantly stimulated by nonpathogenic microorganisms present in the body and thus are already primed.

Furthermore, the IFN response after poliovirus infection was also different among tissues. High-level response was observed in the spleen but was not observed in the spinal cord. This suggests that the IFN response profile may differ depending on the cells and tissues. Since RIG-I and MDA-5/helicard are also IFN inducible (17, 48), they also existed more abundantly in the nontarget tissues (Fig. 6), like other ISGs (Fig. 5). Some of the important regulators of the IFN response, such as IRF-7 and IRF-9, are also IFN inducible. The cells that are primed even at low levels of IFNs may be equipped with all the machinery necessary for the IFN response. Thus, the nontarget tissues may be ready to respond to viral infection. Unequal distribution of the regulators of the IFN response is again consistent with the idea that poliovirus replication is selectively inhibited in nontarget tissues.

On the contrary, neurons in the brainstem and spinal cord could not induce a sufficient antiviral state after poliovirus infection. However, pretreatment with poly(I:C) increased the survival of PVR-transgenic mice against poliovirus challenge (Fig. 7). This suggests that neurons also became resistant to poliovirus infection as long as they were treated. It is therefore possible that the status of ISG expression in the early phase of infection is critical in determining the fate of infected cells and an unequal IFN response may be one of the reasons for the differential susceptibility of cells and tissues to poliovirus. Although the IFN response was not equal in PVR-transgenic mice, both the basal expression of ISGs and induction of ISGs after poliovirus infection are equally null in PVR-transgenic/*Ifnar* knockout mice. Without these unequal protective responses, replication of poliovirus was observed in PVR-transgenic/*Ifnar* knockout mice in the nontarget tissues as well.

Incidence of paralytic disease is influenced by the IFN response. In a natural poliovirus infection, less than 1% of infected individuals develop paralytic disease, and virus clearance occurs in most persons with asymptomatic or mild infections (4, 23, 35). Viremia is observed only transiently in experimentally infected chimpanzees and monkeys, with titers of less than 10^5 tissue culture infective doses per ml with virulent strains (3, 5). Viremia was not observed in a chimpanzee and a human volunteer administered attenuated vaccine strains (35). Thus, viremia titers seem to correlate with central nervous system invasion in primates.

Our data showed that viral replication in visceral tissues is inhibited by the IFN response in PVR-transgenic mice. Poliovirus can enter the central nervous system, penetrating the blood-brain barrier. This pathway is considered the main pathway of poliovirus entry into the central nervous system in the PVR-transgenic mice after poliovirus infection via peripheral routes (47). Inhibition thus results in reduction of the virus titer in the blood and reduction of the chance of virus entry into the central nervous system. In contrast, PVR-transgenic/*Ifnar* knockout mice showed viremia with a very high titer and a high incidence of paralytic disease. It is therefore possible to speculate that the low incidence of paralytic poliomyelitis in humans is also a result of inhibition of poliovirus replication in nonneural tissues by the host IFN response, although we have no experimental evidence on humans. Paralytic poliomyelitis may occur when the alpha/beta IFN response does not work sufficiently in patients with certain conditions. Individuals who have a defect(s) in a gene(s) that contributes to the IFN response would be more susceptible to paralytic poliomyelitis.

Conclusion. The tissue tropism and pathogenesis of viruses are determined by a combination of several factors. In the case of poliovirus infection, poliovirus replication sites are primarily determined by the presence of the receptor, with the capture and entry of the virus into the cells supported by the PVR. Cells expressing PVR at high levels may be favored for poliovirus infection (20). Thus, the tropism of poliovirus may be dependent on the amount of PVR. After virus entry into cells, efficient replication of poliovirus may be dependent on the milieu of infected cells. If the environment is optimal for RNA and viral protein synthesis, a large number of viral particles will be produced per cell. If antiviral activities, such as the IFN response, are sufficiently high, virus replication will be inhibited. Thus, the fate of infected cells is determined by the balance of the replicating capacity of poliovirus and the antiviral activity of the host. Visceral tissues will then fail to serve as a massive factory of poliovirus, and the chance of viral entry into the central nervous system is greatly reduced.

If the virus enters the central nervous system, virulent poliovirus strains can replicate in neurons, where the antiviral defense is not sufficiently ready, and the patient develops paralytic disease. Therefore, the innate antiviral defense is an important determinant of tissue tropism and pathogenicity of poliovirus. It is of interest to investigate if the alpha/beta IFN response also contributes to selective poliovirus infection in the motor neurons in the central nervous system or to infection in the gastrointestinal tract. These questions will be elucidated in future studies. In the case of other viruses, situations such as distribution of the receptor molecule, replication capacity in each tissue, and resistance to the IFN system may differ from those of poliovirus. It therefore seems likely that each virus displays a distinct disease pattern unique to that particular virus.

ACKNOWLEDGMENTS

We thank Masayoshi Kohase, Seii Ohka, Akio Nomoto, Hitoshi Horie, Shinobu Abe, Bunshichi Shimizu, Sou Hashizume, Michiaki Masuda, Masahiko Takada, Eckard Wimmer, and Yoshiyuki Nagai for providing materials, technical assistance, and helpful discussion.

This work was supported in part by a Grant-in-Aid for Scientific Research from the Japanese Ministry of Education, Culture, Sports, Science, and Technology and by a Grant-in-Aid for Research on Emerging and Re-emerging Infectious Diseases from the Japanese Ministry of Health, Labour and Welfare.

REFERENCES

1. **Asada-Kubota, M., T. Ueda, M. Shimada, K. Takeda, and T. Sokawa.** 1995. Distribution of immunoreactive 2′, 5′-oligoadenylate synthetase in mouse digestive tract. J. Interferon Cytokine Res. **15:**863–867.
2. **Bodian, D.** 1949. Histopathologic basis of clinical findings in poliomyelitis. Am. J. Med. **6:**563–578.
3. **Bodian, D.** 1954. Viremia in experimental poliomyelitis. I. General aspects of infection after intravascular inoculation with strains of high and of low invasiveness. Am. J. Hyg. **60:**339–357.
4. **Bodian, D.** 1955. Emerging concept of poliomyelitis infection. Science **12:** 105–108.
5. **Bodian, D.** 1956. Poliovirus in chimpanzee tissues after virus feeding. Am. J. Hyg. **64:**181–197.
6. **Bodian, D., and H. A. Howe.** 1940. An experimental study of the role of neurones in the dissemination of poliomyelitis virus in the nervous system. Brain **63:**135–167.
7. **Chebath, J., P. Benech, M. Revel, and M. Vigneron.** 1987. Constitutive expression of (2′-5′) oligo A synthetase confers resistance to picornavirus infection. Nature **330:**587–588.
8. **Coccia, E. M., G. Romeo, A. Nissim, G. Marzaili, R. Albertini, E. Affabris, A. Battistini, G. Fiorucci, R. Orsatti, G. B. Rossi, and J. Chebath.** 1990. A full-length murine 2-5A synthetase cDNA transfected in NIH-3T3 cells impairs EMCV but not VSV replication. Virology **179:**228–233.
9. **Fiette, L., C. Aubert, U. Mueller, S. Huang, M. Aguet, and M. Brahic, and J.-F. Bureau.** 1995. Theiler's virus infection of 129Sv mice that lack the interferon α/β or interferon γ receptors. J. Exp. Med. **181:**2069–2076.
10. **Garcia-Sastre, A., R. K. Durbin, H. Zheng, P. Palese, R. Gertner, D. E. Levy, and J. E. Durbin.** 1998. The role of interferon in influenza virus tissue tropism. J. Virol. **72:**8550–8558.
11. **Gromeier, M., L. Alexander, and E. Wimmer.** 1996. Internal ribosomal entry site substitution eliminates neurovirulence in intergeneric poliovirus recombinants. Proc. Natl. Acad. Sci. USA **93:**2370–2375.
12. **Henkel, E., S. Morich, and R. Henkel.** 1984. 2-chloro-4-nitrophenyl-β-D-maltoheptaoxide: A new substrate for the determination of α-amylase in serum and urine. J. Clin. Chem. Clin. Biochem. **22:**489–495.
13. **Holland, J. J.** 1961. Receptor affinities as major determinants of enterovirus tissue tropisms in humans. Virology **15:**312–326.
14. **Ida-Hosonuma, M., T. Iwasaki, C. Taya, Y. Sato, J. Li, N. Nagata, H. Yonekawa, and S. Koike.** 2002. Comparison of neuropathogenicity of poliovirus in two transgenic mouse strains expressing human poliovirus receptor with different distribution patterns. J. Gen. Virol. **83:**1095–1105.
15. **Iwasaki, A., R. Welker, S. Mueller, M. Linehan, A. Nomoto, and E. Wimmer.** 2002. Immunofluorescence analysis of poliovirus receptor expression in Peyer's patches of humans, primates, and CD155 transgenic mice: implications for poliovirus infection. J. Infect. Dis. **186:**585–592.
16. **Kakuta, S., S. Shibata, and Y. Iwakura.** 2002. Genomic structure of the mouse 2′, 5′-oligoadenylate synthetase gene family. J. Interferon Cytokine Res. **22:**981–993.
17. **Kang, D.-C., R. V. Gopalkrishnan, Q. Wu, E. Jankowsky, A. M. Pyle, and P. B. Fisher.** 2002. mda-5: An intereferon-inducible putative RNA helicase with double-stranded RNA-dependent ATPase activity and melanoma growth-suppressive properties. Proc. Natl. Acad. Sci. USA **99:**637–642.
18. **Koike, S., H. Horie, I. Ise, A. Okitsu, M. Yoshida, N. Iizuka, K. Takeuchi, T. Takegami, and A. Nomoto.** 1990. The poliovirus receptor protein is produced both as membrane-bound and secreted forms. EMBO J. **9:**3217–3224.
19. **Koike, S., I. Ise, Y. Sato, H. Yonekawa, O. Gotoh, and A. Nomoto.** 1992. A second gene for the African green monkey poliovirus receptor that has no putative N-glycosylation site in the functional N-terminal immunoglobulin-like domain. J. Virol. **66:**7059–7066.
20. **Koike, S., C. Taya, J. Aoki, Y. Matsuda, I. Ise, H. Takeda, T. Matsuzaki, H. Amanuma, H. Yonekawa, and A. Nomoto.** 1994. Characterization of three different transgenic mouse lines that carry human poliovirus receptor gene –influence of the transgene expression on pathogenesis. Arch. Virol. **139:** 351–363.
21. **Koike, S., C. Taya, T. Kurata, S. Abe, I. Ise, H. Yonekawa, and A. Nomoto.** 1991. Transgenic mice susceptible to poliovirus. Proc. Natl. Acad. Sci. USA **88:**951–955.
22. **Mashimo, T., P. Glasser, M. Lucas, D. Simon-Chazottes, P. E. Ceccaldi, X. Montagutelli, P. Despres, and J.-L. Guénet.** 2003. Structural and functional genomics and evolutionary relationship in the cluster of genes encoding murine 2′,5′-oligoadenylate synthetases. Genomics **82:**537–552.
23. **Melnick, J. L.** 1996. Enteroviruses: polioviruses, coxsackieviruses, echoviruses, and newer enteroviruses, p. 655–712. *In* B. N. Fields, D. M. Knipe, and P. M. Howley (ed.) Fields virology, 3rd ed. Lippincott-Raven, Philadelphia, Pa.
24. **Mendelson, C. L., E. Wimmer, and V. R. Racaniello.** 1989. Cellular receptor for poliovirus: molecular cloning, nucleotide sequence, and expression of a new member of the immunoglobulin superfamily. Cell **56:**855–865.
25. **Meurs, E. F., Y. Watanabe, S. Kadereit, G. N. Barber, M. G. Katze, K. Chong, B. R. Williams, and A. G. Hovanessian.** 1992. Constitutive expression of human double-stranded RNA-activated p68 kinase in murine cells mediates phosphorylation of eukaryotic initiation factor 2 and partial resistance to encephalomyocarditis virus growth. J. Virol. **66:**5805–5814.
26. **Müller, U., U. Stainhoff, L. F. Reis, S. Hemmi, J. Pavlovic, R. M. Zinkernagel, and M. Aguet.** 1994. Functional role of type I and II interferons in antiviral defense. Science **264:**1918–1921.
27. **Munoz, A., and L. Carrasco.** 1984. Action of human lymphoblastoid interferon on HeLa cells infected with RNA-containing animal viruses. J. Gen. Virol. **65:**377–390.
28. **Mrkic, B., J. Pavlovic, J., T. Ruelicke, P. Volpe, C. J. Buchholz, D. Hourcade, J. P. Atkinson, A. Aguzzi, and R. Cattaneo.** 1998. Measles virus spread and pathogenesis in genetically modified mice. J. Virol. **72:**7420–7427.
29. **Nomoto, A., S. Koike, and J. Aoki.** 1994. Tissue tropism and species specificity of poliovirus infection. Trends Microbiol. **2:**47–51.
30. **Perelygan, A. A., S. V. Scherbik, I. B. Zhulin, B. M. Stockman, Y. Li, and M. A. Brinton.** 2002. Positional cloning of the murine flavivirus resistance gene. Proc. Natl. Acad. Sci. USA **99:**9322–9327.
31. **Ren, R., F. Constantini, E. J. Gorgacz, J. J. Lee, and V. R. Racaniello.** 1990. Transgenic mice expressing a human poliovirus receptor: a new model for poliomyelitis. Cell **63:**353–362.
32. **Ren, R., and V. R. Racaniello.** 1992. Human poliovirus receptor gene expression and poliovirus tissue tropism in transgenic mice. J. Virol. **66:**296–304.
33. **Rueckert, R.** 1996. Picornaviridae: the viruses and their replication. p. 609–654. *In* B. N. Fields, D. M. Knipe, and P. M. Howley (ed.) Fields virology, 3rd ed. Lippincott-Raven, Philadelphia, Pa.
34. **Ryman, K., W. B. Klimstra, K. B. Nguyen, C. A. Biron, and R. E. Johnston.** 2000. Alpha/beta interferon protects adult mice from fatal Sindbis virus infection and is an important determinant of cell and tissue tropism. J. Virol. **74:**3366–3378.
35. **Sabin, A.** 1956. Pathogenesis of poliomyelitis: reappraisal in light of the new data. Science **123:**1151–1157.
36. **Samuel, C. E.** 1991. Antiviral actions of interferon. Interferon-regulated cellular proteins and their surprisingly selective antiviral activities. Virology **183:**1–11.
37. **Sato, M., H. Suemori, N. Hata, M. Asargiri, K. Ogasawara, K. Nakao, T. Nakaya, M. Katsuki, S. Noguchi, N. Tanaka, and T. Taniguchi.** 2000. Distinct and essential roles of transcription factors IRF-3 and IRF-7 in response to viruses for IFN-α/β gene induction. Immunity **13:**539–548.
38. **Schneider-Schaulies, J.** 2000. Cellular receptors for viruses: link to tropism and pathogenesis. J. Gen. Virol. **81:**1413–1429.
39. **Sen, G. C., and P. Lengyel.** 1992. The interferon system. A bird's eye view of its biochemistry. J. Biol. Chem. **267:**5017–5020.
40. **Shiroki, K., H. Kato, S. Koike, K. Odaka, and A. Nomoto.** 1993. Temperature-sensitive mouse cell factors for strand-specific initiation of poliovirus RNA synthesis. J. Virol. **67:**3989–3991.
41. **Stark, G. R., I. M. Kerr, B. R. G. Williams, R. H. Silverman, and R. D. Schriber.** 1998. How cells respond to interferons. Annu. Rev. Biochem. **67:**227–264.
42. **Tagawa, Y., K. Sekikawa, and Y. Iwakura.** 1997. Suppression of concanavalin A-induced hepatitis in IFN-gamma$^{-/-}$ mice, but not in TNF-alpha$^{-/-}$ mice: role for IFN-gamma in activating apoptosis of hepatocytes. J. Immunol. **159:**1418–1428.
43. **Ueda, T., R. Tatsumi, N. Tanaka, M. Asada-Kubota, K. Hamada, S. Noguchi, T. Taniguchi, and Y. Sokawa.** 1998. Production of immunoreactive 2′,5′-oligoadenylate synthetase in p48-deficient mice. J. Interferon Cytokine Res. **18:**181–185.
44. **Wessely, R., K. Klingel, K. U. Knowlton, and R. Kandolf.** 2001. Cardioselective infection with coxsackievirus B3 requires intact type 1 interferon signaling: implications for mortality and early viral replication. Circulation **103:**765–771.
45. **World Health Organization.** 1990. Manual for the virological investigation of poliomyelitis. World Health Organization, Expanded Programme on Immunization and Division of Communicable Diseases. W.H.O. Publication no. W.H.O./EPI/CDS/POLIO/ 90.1. World Health Organization, Geneva, Switzerland.
46. **Yanagiya, A., S. Ohka, N. Hashida, M. Okamura, C. Taya, N. Kamoshita, K. Iwasaki, Y. Sasaki, H. Yonekawa, and A. Nomoto.** 2003. Tissue-specific replicating capacity of a chimeric poliovirus that carries the internal ribosome entry site of hepatitis C virus in a new mouse model transgenic for the human poliovirus receptor. J. Virol. **77:**10479–10487.
47. **Yang, W. X., T. Terasaki, K. Shiroki, S. Ohka, J. Aoki, S. Tanabe, T. Nomura, E. Terada, Y. Sugiyama, and A. Nomoto.** 1997. Efficient delivery of circulating poliovirus to the central nervous system independently of poliovirus receptor. Virology **17:**421–428.
48. **Yoneyama, M., M. Kikuchi, T. Natsukawa, N. Shinobu, T. Imaizumi, M. Miyagishi, K. Taira, S. Akira, and T. Fujita.** 2004. The RNA helicase RIG-I has an essential function in double-stranded RNA-induced innate antiviral responses. Nat. Immunol. **5:**730–737.
49. **Zhou, A., J. Paranjape, T. L. Brown, H. Nie, S. Naik, B. Dong, A. Chang, B. Trapp, R. Fairchild, C. Colmenares, and R. H. Silverman.** 1997. Interferon action and apoptosis are defective in mice devoid of 2′,5′-oliogoadenylate-dependent RNase L. EMBO J. **16:**6355–6363.

We sequenced a 1,012-bp fragment encompassing the first two thirds of the 16S rDNA of ROG140 (accession no. AY692224). The sequence was compared with those of type strains of all members of the former genus *Micrococcus*, and a phylogenetic tree was deduced by the neighbor–joining method (Figure). The sequences of ROG140 and the *K. schroeteri* type strain only differ by an A-to-G substitution at position 747 (*E. coli* numbering). Among the 21 nucleotide differences between the sequences of *K. schroeteri* and the closely related species *K. sedentarius*, 10 are located on a 30-base stretch and constitute a convenient *K. schroeteri* signature (Figure)

Antimicrobial susceptibility testing performed with the disk diffusion method and Etests (AB Biodisk, Solna, Sweden) indicated that the isolate was resistant to penicillins, cephalosporins, kanamycin, tobramycin, erythromycin, clindamycin, sulfonamides, and fusidic acid, but susceptible to imipenem (MIC, 0.25 μg/mL), gentamicin (MIC, 1 μg/mL), trimethoprim (MIC, 0.25 μg/mL), tetracycline (MIC, 0.12 μg/mL), linezolid (MIC, 0.25 μg/mL), vancomycin (MIC, 0.125 μg/mL), teicoplanin (MIC, 0.06 μg/mL), and rifampicin (MIC, <0.002 μg/mL). Unlike the original isolate reported by Becker et al. (1), isolate ROG140 was resistant to ofloxacin and ciprofloxacin (MICs, 8 μg/mL). Conversely, moxifloxacin displayed excellent in vitro activity (MIC, 0.05 μg/mL). As moxifloxacin was more rapidly microbicidal than vancomycin in an animal model of *Staphylococcus aureus* prosthetic valve endocarditis (4), it might present a potential advantage against infections caused by *K. schroeteri*, especially when the oral route is favored.

The natural habitat of *K. schroeteri* remains unknown. The only isolates of *K. schroeteri* identified so far originated from blood or cardiac material, although *Kytococcus* literally means "a coccus from the skin." Our attempts to recover *K. schroeteri* from the mouth, nose, or skin of our patient were unsuccessful. In a recent study, Szczerba et al. were able to isolate most micrococcal species, including *K. sedentarius* but not *K. schroeteri*, from human skin and mucosa (5). However, at that time the authors may not have been aware of this newly described species. The mode of contamination also remains unclear. In the original description (1), *K. schroeteri* endocarditis had developed in the patient <3 months after she underwent cardiac surgery, which suggested perioperative contamination. Here, we describe a late onset, subacute infection 3 years after surgery, which is more likely to have been caused by hematogenous spread.

Although *Micrococcus*-like organisms cause endocarditis infrequently (6), the description of 2 independent infections due to a new species in a short period is intriguing and suggests a specific pathogenicity, at least on prosthetic heart devices. By demonstrating the presence of the bacteria in the infected site, this report establishes *K. schroeteri* as a genuine pathogen in this clinical setting and should prompt further investigations to identify its natural habitat and virulence determinants. At present, commercial systems are not able to identify *K. schroeteri*. However, gram-positive cocci that are strictly aerobic, oxacillin-resistant, and arginine dihydrolase-positive should be recognized as potential *Kytococcus* species and taken into account when endocarditis is suspected.

Cécile Le Brun,* Julien Bouet,* Philippe Gautier,* Jean-Loup Avril,* and Olivier Gaillot*

*Centre Hospitalier Universitaire de Rennes, Rennes, France

References

1. Becker K, Wüllenweber J, Odenthal HJ, Moeller M, Schumann P, Peters G, et al. Prosthetic valve endocarditis due to *Kytococcus schroeteri*. Emerg Infect Dis 2003;9:1493-4.
2. Becker K, Schumann P, Wüllenweber J, Schulte M, Weil HP, Stackebrandt E, et al. *Kytococcus schroeteri* sp. nov., a novel gram-positive actinobacterium isolated from a human clinical source. Int J Syst Evol Microbiol 2002;52:1609-14.
3. Stackebrandt E, Koch C, Gvozdiak O, Schumann P. Taxonomic dissection of the genus *Micrococcus*: *Kocuria* gen. nov., *Nesterenkonia* gen. nov., *Kytococcus* gen. nov., *Dermacoccus* gen. nov., and *Micrococcus* Cohn 1872 gen. emend. Int J Syst Bacteriol 1995;45:682-92.
4. Entenza JM, Que YA, Vouillamoz J, Glauser MP, Moreillon P. Efficacies of moxifloxacin, ciprofloxacin, and vancomycin against experimental endocarditis due to methicillin-resistant *Staphylococcus aureus* expressing various degrees of ciprofloxacin resistance. Antimicrob Agents Chemother 2001;45:3076-83.
5. Szczerba I, Krzeminski Z. Occurrence and number of bacteria from the *Micrococcus*, *Kocuria*, *Nesterenkonia*, *Kytococcus* and *Dermacoccus* genera on skin and mucous membranes in humans. Med Dosw Mikrobiol 2002;55:67-74.
6. Seifert H, Kaltheuner M, Perdreau-Remington F. *Micrococcus luteus* endocarditis: case report and review of the literature. Zentralbl Bakteriol 1995;282:431-5.

Address for correspondence: Olivier Gaillot, Laboratoire de Bactériologie-Virologie, Faculté de Médecine-Université de Rennes 1, 35033 Rennes, France; fax: + 33 2 99 28 41 59; email: Olivier.Gaillot@univ-rennes1.fr

Viral Gastroenteritis in Mongolian Infants

To the Editor: Viral agents of gastroenteritis affect millions of persons of all ages worldwide (1). The major agents include rotavirus, norovirus, sapovirus, astrovirus, and enteric adenovirus. Rotavirus is the most frequent cause of acute sporadic childhood gastroenteritis (1), whereas norovirus infects both adults and children and is mainly associated with

outbreaks of acute gastroenteritis (1). These viruses are commonly transmitted by foodborne, person-to-person, fecal-oral, and environmental routes.

In 1999, the infant death rate was 37.3 per 1,000 live births in Mongolia (2). Bacterial pathogens, such as *Shigella flexneri* and *Salmonella*, are commonly detected in hospitalized patients with gastroenteritis, but no data exist concerning viral agents of gastroenteritis in hospitalized patients or in the general community (2).

This preliminary community-based molecular epidemiologic study was the first to report viral agents of gastroenteritis in Mongolian infants. Stool specimens collected from July to August 2003 from 36 infants belonging to 25 different households from 2 areas in Mongolia were screened for rotavirus, norovirus, sapovirus, astrovirus, and adenovirus. The 2 areas were Tov Province, which included Zuun Mod (provincial center) and Bayanchandmani (provincial district center), and Ulaanbaatar area (capital city), which included Chingeltei, Bayangol, Songinok-harikhan, and Bayanzurkh. A total of 48 stool specimens, which were randomly selected from negative-enterovirus specimens (poliovirus and nonpolio enterovirus (Minako Kuramitsu, unpub. data), were screened. Of the 36 infants in the study, 2 specimens were collected 3 weeks apart from each of 12 infants, and 1 specimen was collected from each of 24 infants. In 10 households, specimens were collected from 2 or 3 siblings. Clinical symptoms were recorded when available.

RNA extraction, cDNA synthesis, and polymerase chain reaction (PCR) were performed as described elsewhere (3); for norovirus genogroup (G) I (GI), PCR, G1SKF, and G1SKR primers were used, and for norovirus GII PCR, G2SKF, and G2SKR primers were used (4). For sapovirus, a nested PCR approach was used for all human genogroups (5). For the first sapovirus PCR, SV-F11 and SV-R1 primers were used, while for the nested PCR, SV-F21, and SV-R2 primers were used. For astrovirus PCR, Mon244, and 82b primers were used (6). All PCR products were analyzed by 2% agarose gel electrophoresis and visualized by ethidium bromide staining. For rotavirus and adenovirus screening, a rapid dry-spot latex agglutination test, Diarlex Rota-Adeno (Orion Diagnostica, Espo, Finland) was used.

Reverse transcription (RT)–PCR products were excised from the gel and purified by the QIAquick gel extraction kit (Qiagen, Hilden, Germany). Nucleotide sequences were prepared with the terminator cycle sequence kit (version 3.1) and determined with the ABI 3100 avant sequencer (Applied Biosystems, Foster City, CA, USA). Nucleotide sequences were aligned with Clustal X and the distances were calculated by Kimura's 2-parameter method (3). The nucleotide sequence data determined in this study have been deposited in GenBank under accession no. AY590250–AY590262.

Specimens from 12 (33%) of 36 infants were positive for viral agents of gastroenteritis. Specimens from 9 infants were positive for noroviruses, specimens from 2 infants were positive for astroviruses, and a specimen from 1 infant was positive for sapovirus. All specimens were negative for rotavirus and adenovirus. Ten isolated norovirus sequences (9 persons) were classified according to the recent capsid-based sequence scheme of Kageyama et al. (7). Two norovirus sequences belonged to genogroup I/genotype 11 (G1/11), 4 sequences belonged to GII/3, 1 sequence belonged to GII/7, and 3 sequences belonged to GII/6 (Table).

In 1 household, 2 female infants (isolates 213-3 and 214-3, respectively) were infected with a norovirus GI/11 strain that shared 100% nucleotide identity. This strain was

Table. Mongolian infants positive for viral agents of gastroenteritis

Virus	Genogroup/genotype	Specimen*	Symptom†	Age (mo.)	Sex
Norovirus	GI/11	213-3‡	NA	4	F
Norovirus	GI/11	214-3‡	NA	24	F
Norovirus	GII/6	101-1	None	5	F
Norovirus	GII/3	109-1	Diarrhea	6	F
Norovirus	GII/6	205-3	NA	5	F
Norovirus	GII/3	209-1	Diarrhea	3	M
Norovirus	GII/3	317-1§	NA	24	M
Norovirus	GII/6	613-1	None	5	M
Norovirus	GII/7	613-3	NA	5	M
Norovirus	GII/3	609-3§	NA	5	M
Astrovirus	GI	121-3	NA	4	M
Astrovirus	GI	201-3	NA	5	M
Sapovirus	GI	217-1	Diarrhea	1	F

*First 3 numbers before the hyphen refer to the infant; number after the hyphen refers to the week the specimen was collected.
†NA, not available.
‡Two siblings from the same household.
§Only 1 of the siblings from this household was infected.
¶Astrovirus GI = serotype 1.

likely the same and suggests a common source of contamination or person-to-person transmission. Strains belonging to this new genotype have only been detected in Japan and Switzerland (7).

In a different household, 2 different norovirus strains were detected 3 weeks apart in a 5-month-old male infant (isolates 613-1 and 613-3, respectively). These 2 isolated norovirus sequences shared 77.5% nucleotide identity and clustered into two different genotypes, GII/6 (isolate 613-1) and GII/7 (isolate 613-3). In spite of this infection, the infant had no symptoms of gastroenteritis during excretion of the first norovirus strain.

In 4 other households, 4 infants (isolates 109-1, 609-3, 317-1, and 209-1) were infected with norovirus strains belonging to GII/3. These 4 isolated sequences shared >98% nucleotide identity to Arg320 sequence (AF190817), which was previously found to be a recombinant norovirus (8). This result suggests these 4 strains are also recombinant noroviruses, though further sequence analyses of other genetic regions are needed to confirm this result.

Astrovirus was detected in 2 male infants from different households. One infant was 4 months of age (isolate 121-3), and the other infant was 5 months of age (isolate 201-3). These 2 isolated astrovirus sequences had 100% nucleotide identity, which suggests a common source of contamination. These isolated astrovirus sequences shared 98% nucleotide identity to astrovirus Oxford virus sequence (genogroup I). Sapovirus was detected in 1 stool specimen (isolate 217-1) from a 1-year-old female with diarrhea. The isolated sapovirus sequence shared 98% nucleotide identity to sapovirus Manchester virus sequence (genogroup I). Rotavirus and adenovirus were not detected in any of these specimens; further studies, including those of hospitalized infants, may be useful since infants with rotavirus infections are commonly admitted to hospitals (9).

Our preliminary findings have shown that norovirus was a common agent of gastroenteritis (9 of 36 persons) in Mongolian infants. In a recent report on norovirus gastroenteritis, the risk of contracting gastroenteritis was high when another household member was infected and slightly higher when that member was a child (10). In our study, we found 2 siblings infected with an identical norovirus strain during the same period. In Mongolia, diarrhea has become a major healthcare problem (2), therefore, general education in sanitation and hygiene practices may help reduce the transmission of these viruses and lessen the frequency of this disease.

Acknowledgments

We thank the epidemiology team and family doctors of Mongolia for assisting with specimen collections and Peter White for his help with this manuscript.

This work was supported by Grants-in-Aid from the Ministry of Education, Culture, Sports, Science and Technology, Japan, and a Grant for Research on Re-emerging Infectious Diseases from the Ministry of Health, Labor, and Welfare, Japan. Grant Hansman was supported by a Ph.D. scholarship from the Ministry of Health, Labor, and Welfare, Japan.

This work was carried out in the Department of Virology II, National Institute of Infectious Diseases, Tokyo, Japan

Grant Stuart Hansman,*†
Minako Kuramitsu,*
Hiromu Yoshida,†
Kazuhiko Katayama,†
Naokazu Takeda,†
Hiroshi Ushijima,*
Gungaa Surenkhand,‡
Dugerjav Gantulga,‡
and Chushi Kuroiwa*

*University of Tokyo, Tokyo, Japan; †National Institute of Infectious Diseases, Tokyo, Japan; ‡Ministry of Health, Ulaanbaatar, Mongolia

References

1. Wilhelmi I, Roman E, Sanchez-Fauquier A. Viruses causing gastroenteritis. Clin Microbiol Infect. 2003;9:247–62.
2. Ebright JR, Altantsetseg T, Oyungerel R. Emerging infectious diseases in Mongolia. Emerg Infect Dis. 2003;9:1509–15.
3. Hansman GS, Katayama K, Maneekarn N, Peerakome S, Khamrin P, Tonusin S, et al. Genetic diversity of norovirus and sapovirus in hospitalized infants with sporadic cases of acute gastroenteritis in Chiang Mai, Thailand. J Clin Microbiol. 2004;42:1305–7.
4. Kojima S, Kageyama T, Fukushi S, Hoshino FB, Shinohara M, Uchida K, et al. Genogroup-specific PCR primers for detection of Norwalk-like viruses. J Virol Methods. 2002;100:107–14.
5. Okada M, Shinozaki K, Ogawa T, Kaiho I. Molecular epidemiology and phylogenetic analysis of Sapporo-like viruses. Arch Virol. 2002;147:1445–51.
6. Matsui M, Ushijima H, Hachiya M, Kakizawa J, Wen L, Oseto M, et al. Determination of serotypes of astroviruses by reverse transcription-polymerase chain reaction and homologies of the types by the sequencing of Japanese isolates. Microbiol Immunol. 1998;42:539–47.
7. Kageyama T, Shinohara M, Uchida K, Fukushi S, Hoshino FB, Kojima S, et al. Coexistence of multiple genotypes, including newly identified genotypes, in outbreaks of gastroenteritis due to Norovirus in Japan. J Clin Microbiol. 2004;42:2988–95.
8. Jiang X, Espul C, Zhong WM, Cuello H, Matson DO. Characterization of a novel human calicivirus that may be a naturally occurring recombinant. Arch Virol. 1999;144:2377–87.
9. Doan LT, Okitsu S, Nishio O, Pham DT, Nguyen DH, Ushijima H. Epidemiological features of rotavirus infection among hospitalized children with gastroenteristis in Ho Chi Minh City, Vietnam. J Med Virol. 2003;69:588–94.
10. de Wit MA, Koopmans MP, van Duynhoven YT. Risk factors for norovirus, Sapporo-like virus, and group A rotavirus gastroenteritis. Emerg Infect Dis. 2003;9:1563–70.

Address for correspondence: Chushi Kuroiwa, Graduate School of Medicine, International Health Policy and Planning, University of Tokyo, 7-3-1, Hongo, Bunkyo-ku, 113-0033, Tokyo, Japan; fax: 81-3-5841-3637; email: ckuroiw@m.u-tokyo.ac.jp

Behavioral/Systems/Cognitive

Organization of Multisynaptic Inputs from Prefrontal Cortex to Primary Motor Cortex as Revealed by Retrograde Transneuronal Transport of Rabies Virus

Shigehiro Miyachi,[1,2] Xiaofeng Lu,[3] Satoshi Inoue,[4] Takuya Iwasaki,[5] Satoshi Koike,[1] Atsushi Nambu,[6] and Masahiko Takada[1,2]

[1]Tokyo Metropolitan Institute for Neuroscience, Fuchu, Tokyo 183-8526, Japan, [2]Core Research for Evolutional Science and Technology, Japan Science and Technology Agency, Kawaguchi 332-0012, Japan, [3]Department of Physiology, Juntendo University School of Medicine, Tokyo 113-8421, Japan, [4]National Institute of Infectious Diseases, Tokyo 162-8640, Japan, [5]Institute of Tropical Medicine, Nagasaki University, Nagasaki 852-8523, Japan, and [6]National Institute for Physiological Sciences, Okazaki 444-8585, Japan

The organization of multisynaptic projections from the prefrontal cortex to the primary motor cortex (MI) was examined in macaque monkeys by retrograde transneuronal transport of rabies virus. In the first series of experiments, the virus was injected into the MI forelimb region, and the time-dependent distribution patterns of transsynaptic labeling were analyzed in the frontal lobe with various survivals (2–4 d). Two days after the viral injection, neuronal labeling emerged in the caudal aspects of the nonprimary motor-related areas that are known to project to the MI directly. At the same time, the motor thalamus contained labeled neurons. On the third day, cortical labeling extended into the rostral motor-related areas and, also, prearcuate area 8. Moreover, a number of labeled neurons were located in the internal pallidum and the cerebellar nuclei. At the 4 d postinjection period, neuronal labeling occurred widely in prefrontal areas as well as in the putamen and the cerebellar cortex. In the second series of experiments, the viral injection was made into the MI hindlimb region, and the distribution pattern of prefrontal labeling on the fourth day was compared with that in the forelimb-injection case. The labeled neurons in each prefrontal area were much fewer in the hindlimb-injection case than in the forelimb-injection case. Whereas ventral area 46 was most densely labeled from the forelimb region, only sparse labeling from the hindlimb region was observed in this prefrontal area. The present results suggest the importance of ventral area 46 in the cognitive control of forelimb movements.

Key words: prefrontal cortex; primary motor cortex; cortical motor-related areas; somatotopy; basal ganglia; cerebellum

Introduction

The frontal lobe plays crucial roles in the execution and control of various motor behaviors in humans and nonhuman primates. The primary motor cortex (MI), lying in the caudalmost portion of the lobe, has massive projections to the spinal cord in a strict somatotopic manner (He et al., 1993; Galea and Darian-Smith, 1994; Dum and Strick, 1996). This implies the involvement of the MI in the precise control of somatic movements (Georgopoulos et al., 1982; Kakei et al., 1999). In the primate MI, forelimb representation occupies a large sector in the precentral gyrus, thus reflecting the importance of forelimb movements compared with the movements of other body parts. On the other hand, located at the rostral pole of the frontal lobe is the prefrontal cortex that consists of multiple, anatomically distinct areas. These prefrontal areas receive inputs from the parietal association, temporal association, and limbic-related cortical areas (Barbas and Mesulam, 1985; Barbas, 1988; Pandya and Yeterian, 1990; Carmichael and Price, 1995a) and, in turn, send outputs to the frontal motor-related areas (Barbas and Pandya, 1987; Luppino et al., 1993; Lu et al., 1994). It has been proposed that individual areas of the prefrontal cortex play differential roles in the control of voluntary actions according to distinct types of sensory and emotional information. For example, the dorsolateral prefrontal cortex has been implicated in motor selection based on visual information (Wilson et al., 1993; Sakagami and Tsutsui, 1999), whereas the medial prefrontal cortex seems to have certain roles in reward- or context-dependent motor selection (Paus, 2001; Matsumoto et al., 2003). The orbitofrontal cortex is suggested to participate in the reward-dependent control of motor behaviors (Tremblay and Schultz, 1999; Hikosaka and Watanabe, 2000). However, the somatotopic delineation of these prefrontal areas remains unknown. Which prefrontal areas are more strongly involved in motor actions involving the forelimb? So far, it has been difficult to elucidate the pattern of somatotopic representations in the prefrontal cortex. One possible reason is that body part movements cannot be evoked by electrical stimulation in the prefrontal cortex, nor can responses to somatosensory stimuli be elicited

Received May 12, 2004; revised Dec. 7, 2004; accepted Dec. 10, 2004.

This work was supported by Grants-in-Aid for Scientific Research (B) and for Scientific Research on Priority Areas from the Ministry of Education, Culture, Sports, Science and Technology of Japan. We are grateful to Etsuko Mine for technical assistance.

Correspondence should be addressed to Dr. Shigehiro Miyachi, Department of System Neuroscience, Tokyo Metropolitan Institute for Neuroscience, Tokyo Metropolitan Organization for Medical Research, 2-6 Musashidai, Fuchu, Tokyo 183-8526, Japan. E-mail: miyachi@tmin.ac.jp.

DOI:10.1523/JNEUROSCI.4186-04.2005

 0270-6474/05/252547-10$15.00/0

in the prefrontal cortex. In addition, neuronal linkage between the prefrontal cortex and the MI is not well understood, because these two structures are interconnected indirectly by way of nonprimary motor-related areas. To address the issue on the somatotopic aspect of the prefrontal cortex in motor control, it is necessary to analyze the multisynaptic connections between the prefrontal cortex and the MI. For this purpose, transneuronal transport of a neurotropic virus is a useful tool. Rabies virus is known to label neurons through synapses in the retrograde direction (Ugolini, 1995; Kelly and Strick, 2000). In the present study, the virus was injected into forelimb representation of the monkey MI, and the time-dependent distributions of transsynaptic labeling were examined in the frontal lobe with varying survivals (2–4 d). The viral injection was further made into hindlimb representation of the MI, and the pattern of prefrontal labeling was compared with that in the forelimb-injection case.

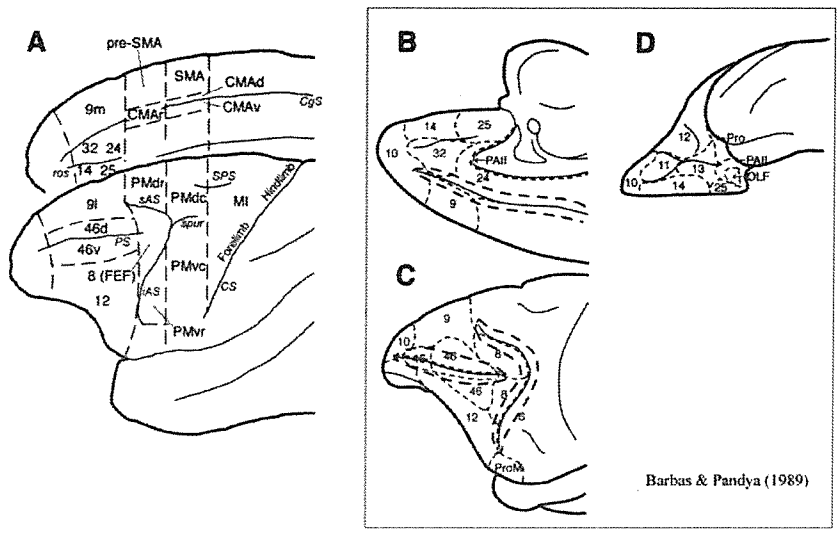

Figure 1. Parcellation of the macaque frontal cortex. *A*, Classification of the prefrontal and motor-related areas used in the present study. *B–D*, Classification of Barbas and Pandya [(1989), their Fig. 2*A–C*, reprinted with permission]. CgS, Cingulate sulcus; CS, central sulcus; iAS, inferior limb of the arcuate sulcus; OLF, olfactory cortex; PAll, limbic periallocortex; Pro, proisocortex; ProM, rostral portion of the ventral premotor cortex; PS, principal sulcus; ros, rostral sulcus; sAS, superior limb of the arcuate sulcus; SPS, superior precentral sulcus; spur, spur of the arcuate sulcus; 8, area 8; 9l, lateral area 9; 9m, medial area 9; 46d, dorsal area 46; 46v, ventral area 46. Numbers correspond to the area numbers defined by Barbas and Pandya (1989).

Materials and Methods

Experimental animals. Ten macaque monkeys (six Japanese and four rhesus monkeys) of either sex weighing 5.5–14 kg were used in this study (see Table 1). Throughout the experimental sessions, the monkeys were kept in individual cages placed inside a special safety cabinet. Food and water were available *ad libitum* in each cage. The experimental protocol was approved by the Animal Care and Use Committee of the Tokyo Metropolitan Institute for Neuroscience (Fuchu, Tokyo, Japan), and all experiments were conducted according to the Tokyo Metropolitan Institute for Neuroscience *Guidelines for the Care and Use of Animals* (2000).

Virus. A stock virus suspension of the challenge-virus-standard (CVS-11) strain was prepared by using mouse neuroblastoma cells of A/J (H-2a) as described previously (Smith et al., 1996). This rabies strain was the same as introduced by Ugolini (1995) and Kelly and Strick (2000) to demonstrate specific retrograde transneuronal transport of the virus. The titer of the stock virus suspension was 1.4×10^8 focus-forming units (FFU)/ml. The virus was derived from the Center for Disease Control and Prevention (Atlanta, GA) and amplified at the National Institute of Infectious Diseases (Tokyo, Japan). A viral suspension was kept in small aliquots at −80°C. Each aliquot was thawed in a safety cabinet just before each injection experiment.

Surgical procedures and electrophysiological mapping. For electrophysiological mapping and the subsequent viral injections, a head holder was surgically attached to the monkey's skull under aseptic conditions. The monkeys were sedated with an intramuscular injection of ketamine hydrochloride (5 mg/kg), anesthetized with an intravenous injection of sodium pentobarbital (20 mg/kg), and then positioned in a stereotaxic apparatus. The head holder was fixed on the skull with anchor screws and dental acrylic resin. After recovery periods of several days, the monkeys were anesthetized with an intramuscular injection of ketamine hydrochloride (5–10 mg/kg) and xylazine hydrochloride (0.5–1 mg/kg) and seated in a primate chair with their head fixed in a stereotaxic frame attached to the chair. After partial removal of the skull over the frontal lobe, the precentral gyrus corresponding to the MI was mapped by intracortical microstimulation. A glass-coated elgiloy-alloy microelectrode (0.5–1.5 MΩ at 1 kHz) attached to a manipulator was inserted perpendicular to the dural surface. When trains of 12 cathodal pulses (200 μs duration at 333 Hz; currents of <50 μA) were delivered through a constant-current stimulator, evoked movements of different body parts were carefully examined. To preserve the exposed dural surface, a rectangular chamber was fixed on the skull with acrylic resin.

Viral injection. A few days after the MI mapping, the monkeys received viral injections into the forelimb or hindlimb region of the MI. Under

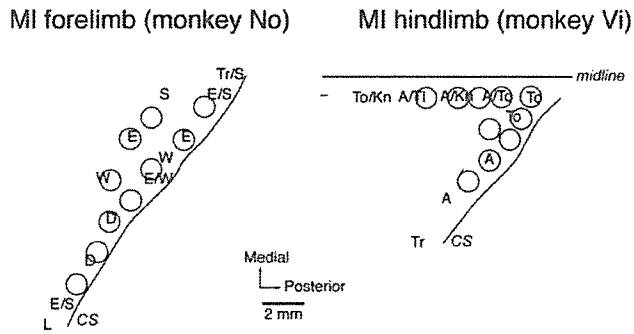

Figure 2. Results of intracortical microstimulation (ICMS) mapping and the sites of rabies virus injection in forelimb (monkey No) or hindlimb (monkey Vi) representation of the MI. Each letter on the cortical surface map denotes the site of electrode penetration, stimulation of which elicited movement predominantly from one of the following body parts: A, Ankle; D, digit (hand); E, elbow; Kn, knee; L, lip; S, shoulder; Tl, tail; To, toe; Tr, trunk; W, wrist; —, locus in which no body movements were elicited by ICMS. Circles indicate the approximate extents of the injection sites. CS, Central sulcus.

Table 1. Summary of experiments

Monkey	Species	Sex	Injection site	Survival (days)	Injection volume (μl)
Ma	J	F	Forelimb	2	8.5
Hu	J	M	Forelimb	3	8
Ke	J	F	Forelimb	3	9
Ir	J	F	Forelimb	3.5	10
Ta	R	M	Forelimb	3.5	9
No	J	M	Forelimb	4	8.5
Ji	R	M	Forelimb	4	10
Qu	R	M	Hindlimb	3	8
Ri	R	M	Hindlimb	4	9
Vi	J	F	Hindlimb	4	10

F, Female; J, Japanese monkey (*Macaca fuscata*); M, male; R, rhesus monkey (*Macaca mulatta*).

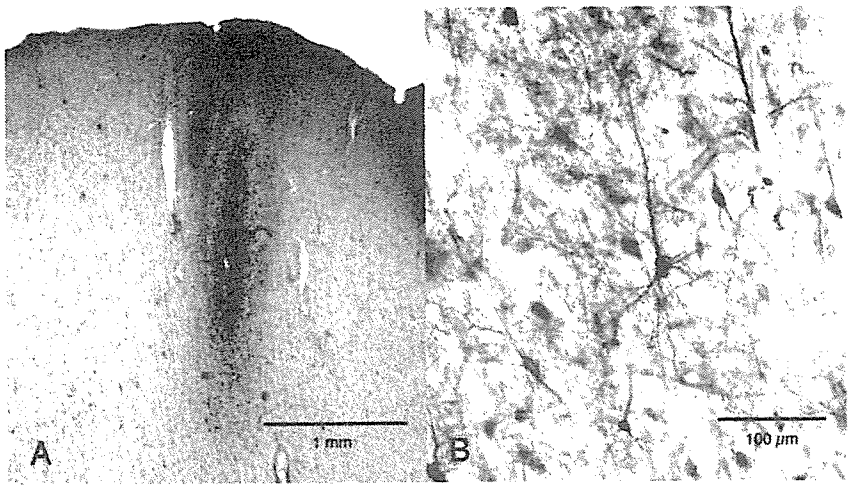

Figure 3. Low- and high-magnification photomicrographs of the injection site in monkey Ma (2 d after the viral injection). In the low-power image (*A*), clusters of labeled neurons are seen around the injection needle track, and in the high-power image (*B*), many neurons are labeled in a Golgi-like manner.

general anesthesia with ketamine hydrochloride (5–10 mg/kg, i.m.) and xylazine hydrochloride (0.5–1 mg/kg, i.m.), each monkey was set in the primate chair in the same manner as in the mapping. A total of 8–10 μl (0.5–1 μl per penetration) of the viral suspension was injected into the identified forelimb or hindlimb region of the MI through a 10 μl Hamilton microsyringe.

Histological procedures. After survival periods of 2–4 d, the monkeys were anesthetized deeply with sodium pentobarbital (50 mg/kg) and perfused transcardially with 0.1 M PBS, pH 7.4, followed by a mixture of 8% formalin and 15% saturated picric acid in 0.1 M phosphate buffer (PB), pH 7.4. The brains were removed from the skull, postfixed in the same fresh fixative overnight, and immersed in PB containing 30% sucrose. Coronal sections were cut serially at 60 μm thickness on a freezing microtome. Every sixth section was immunohistochemically stained for rabies virus with the standard avidin–biotin–peroxidase complex (ABC) method. The detection of rabies virus was performed using a monospecific rabbit antiserum prepared by immunization of His-tagged recombinant nucleoprotein expressed in *Escherichia coli* (Inoue et al., 2003).

The sections were washed briefly in PBS, soaked with 1% skim milk in PBS for 2 h, and then incubated overnight with the primary antibody (diluted at 1:10,000) in PBS containing 0.1% Triton X-100 and 1% normal goat serum. Subsequently, the sections were incubated for 2 h in the same fresh medium containing biotinylated goat anti-rabbit IgG antibody (diluted at 1:200; Vector Laboratories, Burlingame, CA) and reacted with the ABC kit (ABC Elite; Vector Laboratories). For visualization of the antigen, the sections were reacted in 0.05 M Tris-HCl buffer, pH 7.6, containing 0.04% diaminobenzidine, 0.04% nickel chloride, and 0.002% hydrogen peroxide. After washes in PBS, the sections were mounted onto gelatin-coated glass slides. A series of the adjacent sections (60 μm apart) were mounted and Nissl stained with 1% Neutral red or cresyl violet. The areal boundaries in the frontal lobe were determined primarily based on cytoarchitectonic criteria. For the nomenclature of the prefrontal and motor-related areas, the classification of Barbas and Pandya (1987, 1989) was adopted with some modifications (Fig. 1). The caudal and rostral parts of the dorsal premotor cortices (PMdc and PMdr) in the present paper correspond to area 6DC or 6DR, respectively. Whereas the caudal part of the ventral premotor cortex (PMvc) includes area 4C and the caudal part of area 6Va (caudal to the genu of the arcuate sulcus), the rostral part of the ventral premotor cortex (PMvr) includes the rostral part of area 6Va and area 6Vb (rostral to the genu of the arcuate sulcus).

Data analysis. According to electrophysiological mapping data, we prepared the somatotopic map of the MI, which was viewed from the cortical surface. The injection sites of rabies virus in the MI were charted in tracings of equidistant coronal sections and reconstructed on the map. Neuronal labeling in the frontal cortex, the basal ganglia, and the cerebellum was plotted on tracings of representative coronal sections, whereas that in the thalamus was plotted on photomicrographs of corresponding Nissl-stained sections. The number of labeled neurons in each area of the frontal lobe was counted in every 12th section (720 μm apart) by visual inspection under a light microscope. In addition, the distributions of retrograde labeling in the prefrontal cortex in monkeys No and Vi were reconstructed on the unfolded cortical maps. All the unfolded lines were aligned at the fundus of the principal sulcus or, caudally, at the midpoint between the superior and the inferior limb of the arcuate sulcus (Barbas and Pandya, 1987; Hatanaka et al., 2001).

Safety issues. All experiments were performed in a special laboratory (biosafety level 2) designated for *in vivo* virus experiments. Throughout the experiments, the monkeys were kept in individual cages that were placed in the laboratory. To avoid accidental infection with the virus, all investigators received immunization before the present series of experiments and wore protective clothes during the experimental procedures, including viral injection, feeding, and perfusion. Equipment was disinfected with 70% ethanol after each experimental session. Waste was autoclaved before disposal.

Results

Injection sites of rabies virus in forelimb and hindlimb representations of MI

In 10 monkeys, multiple injections of rabies virus were made into forelimb or hindlimb representation of the MI that had been identified electrophysiologically (Fig. 2, Table 1). Seven monkeys received the viral injections into the MI forelimb region and were allowed to survive for 2 d (monkey Ma), 3 d (monkeys Hu and Ke), 3.5 d (monkeys Ir and Ta), or 4 d (monkeys No and Ji). On the other hand, the remaining three monkeys received the viral injections into the MI hindlimb region and were allowed to survive for 3 d (monkey Qu) or 4 d (monkey Ri and Vi). At the 2 d survival period, accumulations of labeled neurons were observed around the needle track of each injection site (Fig. 3*A*). For many labeled neurons, not only their cell bodies but also their dendritic trees were clearly visible (Fig. 3*B*). At the 3–4 d survival periods, dense cell labeling of the injection sites extended for hundreds of micrometers in diameter from the needle tracks. With the different postinjection periods, the distribution patterns of retrograde labeling were analyzed in the frontal lobe, in comparison with those in the basal ganglia and the cerebellum.

On day 2 after viral injection into MI forelimb region

Two days after the viral injection into the forelimb region of the MI, considerable retrograde labeling occurred in the caudal aspects of the nonprimary motor-related areas, which consist of the dorsal and ventral cingulate motor areas (CMAd and CMAv), the supplementary motor area (SMA), and the PMdc and PMvc (see Figs. 1, 4, 7). In contrast, only a small number of labeled neurons were found more rostrally in the frontal lobe (see Fig. 7). At the 2 d postinjection period, many neurons were labeled in the motor thalamus, including the oral division of the ventrolateral nucleus (VLo) and the oral division of the ventroposterolateral nucleus (VPLo) (Fig. 4*I–K*). Some labeled neurons were further observed in other thalamic nuclei, such as the reticular nucleus, the center median

nucleus, and the centrolateral nucleus. More rostrally, labeled neurons were also observed in the basal forebrain (i.e., the substantia innominata; data not shown). However, virtually no neuronal labeling was seen in either the basal ganglia or the cerebellum.

On day 3 after viral injection into MI forelimb region

Three days after the viral injection into the MI forelimb region, many more neurons were labeled in the caudal motor-related areas (see Fig. 7). In addition, areas of dense neuronal labeling in the frontal lobe extended into the rostral aspects of the nonprimary motor-related areas such as the rostral cingulate motor area (CMAr), the presupplementary motor area (pre-SMA), and the PMdr and PMvr (see Figs. 1, 5, 7). On the same day, a number of labeled neurons were also found in prearcuate area 8, corresponding to the frontal eye field (FEF) (Huerta et al., 1987). However, only a few labeled neurons were scattered in the prefrontal cortex. Subcortically, neuronal labeling occurred in both the basal ganglia and the cerebellum (data not shown). The labeled neurons in the basal ganglia were located in the internal segment of the globus pallidus (GPi) ipsilateral to the injection site and, further, in the ventral striatum (Kelly and Strick, 2004). In the cerebellum, the labeled neurons were located in the cerebellar nuclei, especially in the dentate nucleus, contralateral to the injection site.

On days 3.5 and 4 after viral injection into MI forelimb region

On day 3.5 after the viral injection into the MI forelimb region, the rostral motor-related areas were much more densely labeled (see Fig. 7). Likewise, neuronal labeling in the FEF became more prominent. At the 3.5 d postinjection period, a substantial number of labeled neurons was seen in many areas of the prefrontal cortex. These areas extensively involved areas 24/32 and medial area 9 on the medial wall, lateral area 9 and dorsal area 46 on the dorsolateral surface, ventral area 46 and area 12 on the ventrolateral surface, and areas 11/13 and 14/25 in the ventral aspect (see Fig. 7; for their cytoarchitectonic divisions, see Fig. 1). In each of the prefrontal areas, the number of labeled neurons was greatly increased 4 d after the viral injection (Figs. 6, 7). Among the prefrontal areas, ventral area 46 was most densely labeled, and, also, dense clusters of labeled neurons were distributed in area 12 and the medial wall areas (i.e., areas 24/32 and medial area 9). Our quantitative analysis revealed that the density of labeled neurons in the frontal lobe, especially in the rostral motor-related and prefrontal areas, went up exponentially at a rate of ~100 times per day (Fig. 7*B*).

Moreover, a large number of labeled neurons was located in the basal ganglia and the cerebellum at the postinjection periods of 3.5 and 4 d. Neuronal labeling in the basal ganglia was observed not only in the GPi and the ventral striatum but also in the putamen, the external segment of the globus pallidus, and the subthalamic nucleus (Fig. 6*L*). In the cerebellar nuclei, the labeled neurons were found predominantly in the dentate nucleus and, to a lesser extent, in the interpositus nuclei (Fig. 6*M*). Especially at the 4 d postinjection period, Purkinje cells in the cerebellar cortex were labeled to some extent (Fig. 6*M*).

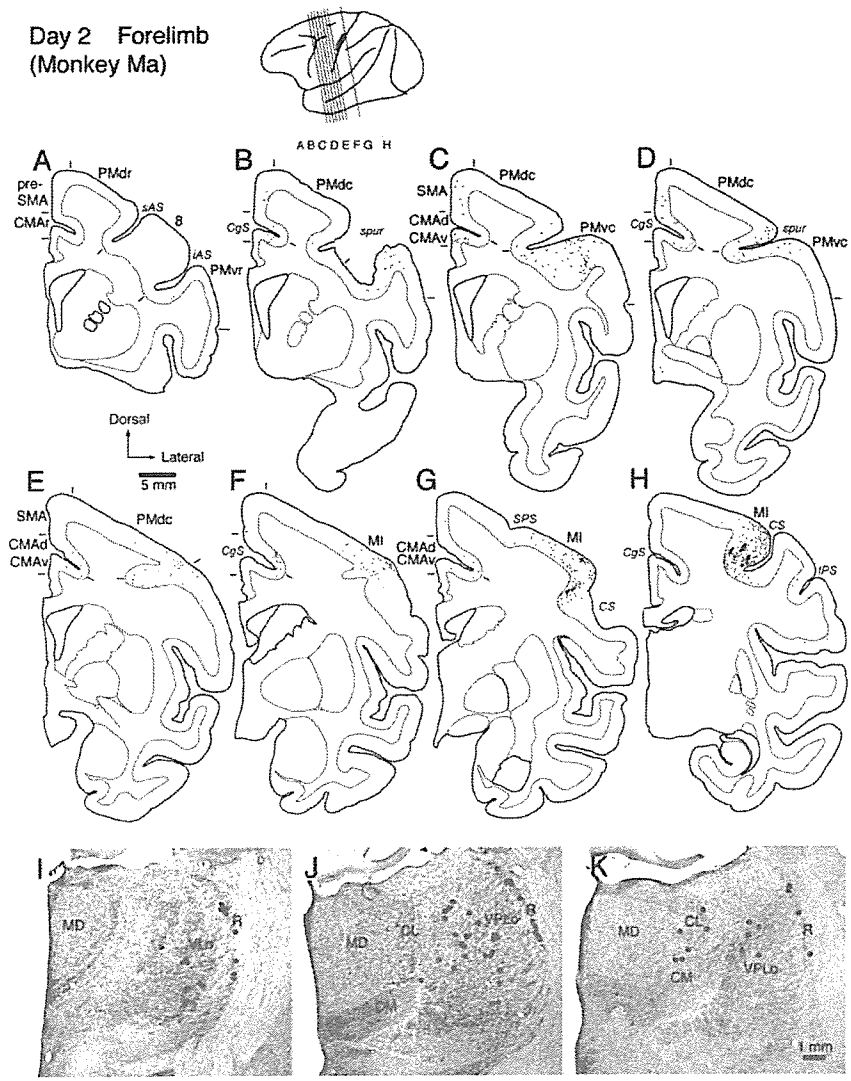

Figure 4. Distribution patterns of retrograde labeling in the frontal lobe (*A–H*) and the thalamus (*I–K*) 2 d after the viral injection into the MI forelimb region (monkey Ma). Eight representative coronal sections through the motor-related areas are arranged rostrocaudally in *A–H*. The approximate rostrocaudal levels of the sections are indicated in the lateral view of the brain. The dark area in this view specifies the extent of the injection site. Photomicrographs of three representative coronal sections through the motor thalamus are arranged rostrocaudally in *I–K*. Each dot in the cortex or the thalamus corresponds to two labeled cells or one labeled cell, respectively. CL, Centrolateral nucleus of the thalamus; CM, center median nucleus of the thalamus; CgS, cingulate sulcus; CS, central sulcus; iAS, inferior limb of the arcuate sulcus; IPS, intraparietal sulcus; MD, mediodorsal nucleus of the thalamus; R, reticular nucleus of the thalamus; sAS, superior limb of the arcuate sulcus; SPS, superior precentral sulcus; spur, spur of the arcuate sulcus; 8, area 8.

Differential distributions of neuronal labeling from forelimb versus hindlimb regions of MI

When the virus was injected into the hindlimb region of the MI, many neurons were retrogradely labeled in the frontal motor-related areas with survivals of 3 and 4 d. At the 3 d postinjection

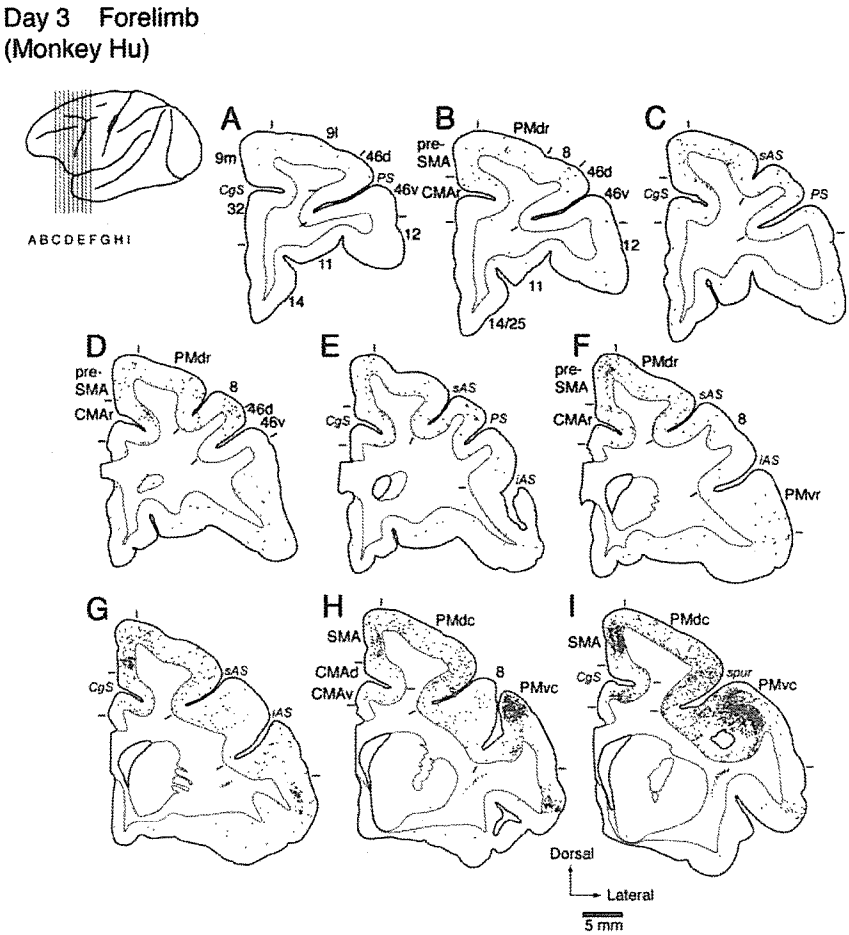

Figure 5. Distribution patterns of retrograde labeling in the frontal lobe 3 d after the viral injection into the MI forelimb region (monkey Hu). Nine representative coronal sections through the motor-related areas and the prefrontal cortex (*A–I*) are arranged rostrocaudally. The approximate rostrocaudal levels of the sections are indicated in the lateral view of the brain. The dark area in this view specifies the extent of the injection site. Each dot corresponds to two labeled cells. CgS, Cingulate sulcus; iAS, inferior limb of the arcuate sulcus; PS, principal sulcus; sAS, superior limb of the arcuate sulcus; spur, spur of the arcuate sulcus; 9l, lateral area 9; 9m, medial area 9; 46d, dorsal area 46; 46v, ventral area 46. Numbers correspond to the area numbers defined by Barbas and Pandya (1989).

period, neuronal labeling was seen abundantly in the caudal motor-related areas. The labeled neurons were distributed mainly in the CMAd and CMAv around the cingulate sulcus and the PMdc medial to the superior precentral sulcus (data not shown). At the 4 d postinjection period, the rostral motor-related areas contained a large number of labeled neurons, especially in the CMAr and PMdr (Fig. 8*C–F*). Neuronal labeling in the prefrontal cortex was also clearly observed (Fig. 8*A*,*B*). The total number of prefrontal neurons labeled from the MI hindlimb region (mean for two monkeys, 3648 cells counted in every 12th section) was 10 times smaller than that in the forelimb-injection case (mean, 38000 cells), although the injected sites in each region covered almost comparable cortical areas (Figs. 2, 9). In addition, the distribution pattern of the labeled neurons from the hindlimb region was different from the distribution pattern of those from the forelimb region (Figs. 9, 10). After the viral injection into the MI hindlimb region, many labeled neurons were located in area 12 and the medial wall areas (i.e., areas 24/32 and medial area 9). Other prefrontal areas exhibited sparse neuron labeling. Of particular interest was that only a few labeled neurons were found in ventral area 46 that was most densely labeled from the MI forelimb region (Figs. 9, 10). Similar findings were obtained in the FEF (i.e., prearcuate area 8). Although strong labeling of FEF neurons was seen 4 d after the viral injection into the MI forelimb region, the FEF was essentially devoid of labeled neurons (Figs. 8, 9).

On days 3 and 4 after the viral injection into the MI hindlimb region, neuronal labeling was evident in the basal ganglia on the same side and in the cerebellum on the opposite side. Especially at the postinjection period of 4 d, dense clusters of labeled neurons in the pallidal complex and the putamen were observed more dorsally than those seen after the injection into the MI forelimb region (compare Figs. 6*L*, 8*I*). The distribution pattern in the putamen of neuronal labeling from the forelimb and hindlimb regions was in good accordance with the topography of corticostriatal terminals from these MI regions (Flaherty and Graybiel, 1993; Takada et al., 1998; Kelly and Strick, 2004). The labeled neurons in the cerebellar nuclei (i.e., the dentate and interpositus nuclei) were distributed predominantly in their rostral portions, whereas those in the forelimb-injection case were distributed more caudally (compare Figs. 6*M*, 8*K*). At the 4 d postinjection period, a number of Purkinje cells were labeled more rostrally in the cerebellar cortex than those in the forelimb-injection case (compare Figs. 6*M*, 8*J*). Thus, our findings revealed that the somatotopic arrangement (forelimb vs hindlimb) of the basal ganglia and the cerebellum was in favor of the previously reported patterns (Hoover and Strick, 1999; Dum and Strick, 2003; Kelly and Strick, 2003, 2004).

Discussion

To use rabies virus for visualization of multisynaptic connections, it is crucial to determine the specificity and rate of transneuronal labeling. For this purpose, we first examined the time-dependent spread of subcortical labeling after viral injections into the MI forelimb region. Consistent with the results of the studies of Kelly and Strick (2003, 2004), neuronal labeling occurred sequentially along the known cortico-basal ganglia and cortico-cerebellar pathways. Two days after the injection, thalamic neurons were labeled mainly in the VLo and VPLo that project to the MI directly. Relatively sparse labeling of these thalamic neurons indicates that a little longer time than 2 d may be needed for sufficient labeling of first-order neurons (for comparison with conventional tracing, see Holsapple et al., 1991; Shindo et al., 1995). At a 3 d postinjection period, both the GPi and the cerebellar nuclei contained labeled neurons. On the fourth day, neuronal labeling in the putamen and the cerebellar cortex became prominent. These results suggest that it takes ~2 d for first-order neuron labeling and 1 additional day per synapse for the subsequent transneuronal labeling. It should be noted, however, that the time course of transneuronal labeling seems somewhat different among neuron types, as shown in the rat brainstem (Ugolini, 1995). For example, reticular thalamic neurons that have no direct projection to the MI were labeled at a 2 d survival. This may

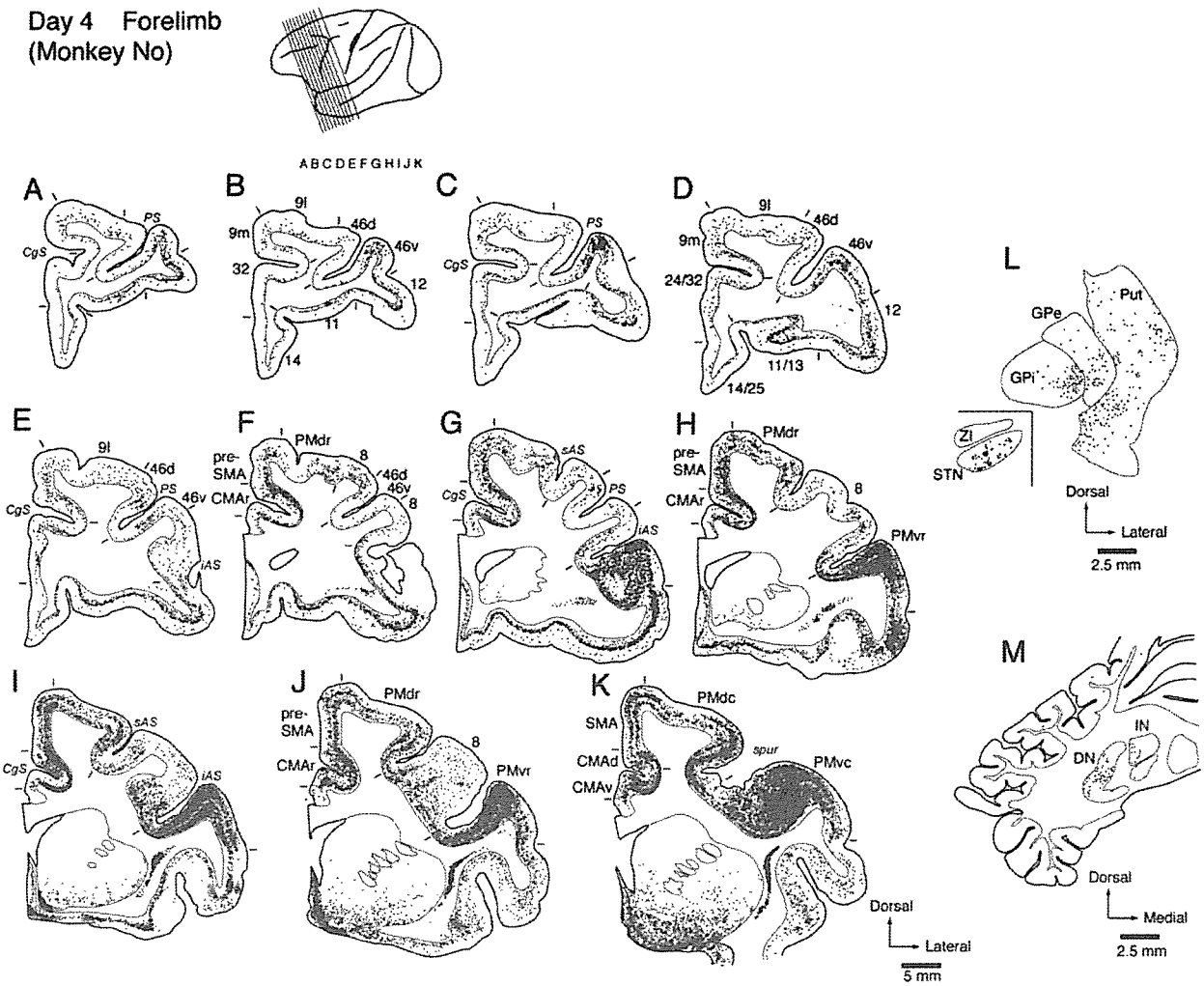

Figure 6. *A–K*, Distribution patterns of retrograde labeling in the frontal lobe 4 d after the viral injection into the MI forelimb region (monkey No). Eleven representative coronal sections through the prefrontal cortex are arranged rostrocaudally (sections *G–J* represent the levels of the rostral motor-related areas). The approximate rostrocaudal levels of the sections are indicated in the lateral view of the brain. The dark area in this view specifies the extent of the injection site. *L*, *M*, Distribution patterns of retrograde labeling in the basal ganglia (*L*) and the cerebellum (*M*). In *L*, clusters of labeled neurons in the internal and external segments of the globus pallidus (GPe) and the putamen (Put) are distributed mainly in their ventral or ventrolateral portions. Note that another cluster of labeled neurons is located far ventromedially within the putamen (Kelly and Strick, 2004). In *A–M*, each dot corresponds to two labeled cells. CgS, Cingulate sulcus; DN, cerebellar dentate nucleus; iAS, inferior limb of the arcuate sulcus; IN, cerebellar interpositus nucleus; PS, principal sulcus; sAS, superior limb of the arcuate sulcus; spur, spur of the arcuate sulcus; STN, subthalamic nucleus; ZI, zona incerta; 9l, lateral area 9; 9m, medial area 9; 46d, dorsal area 46; 46v, ventral area 46. Numbers correspond to the area numbers defined by Barbas and Pandya (1989).

be attributable to exceptionally fast labeling of second-order neurons through the VLo and VPLo, because it has been reported that those neurons are readily labeled in a transsynaptic manner (Itoh et al., 1984). Furthermore, striatal projection neurons tended to be more readily labeled as third-order neurons than cerebellar Purkinje cells. On the other hand, neuronal labeling in the ventral striatum may possibly be attributed to second-order labeling via cholinergic neurons in the basal forebrain that project to the MI monosynaptically, because the basal forebrain labeled initially at a 2 d survival receives input from the ventral striatum, in which labeled neurons were found at a 3 d survival (Haber et al., 1990).

In the frontal cortex, retrograde labeling at a 2 d postinjection period occurred in the caudal motor-related areas, the PMdc, PMvc, SMA, CMAd, and CMAv, that send projection fibers directly to the MI (Muakkassa and Strick, 1979; Tokuno and Tanji, 1993; Hatanaka et al., 2001). At this stage, neurons in the rostral motor-related areas were only sparsely labeled, although part of the areas (i.e., the CMAr) has relatively weak projections to the MI (Dum and Strick, 1991; Takada et al., 2004). On the third day, substantial neuronal labeling extended over the rostral motor-related areas, including the PMdr, PMvr, pre-SMA, and CMAr. Because these areas were labeled simultaneously with the GPi and the cerebellar nuclei, the labeled neurons may probably correspond to second-order neurons. Likewise, many of the labeled neurons in the prefrontal cortex can be considered third-order neurons, because conspicuous labeling of striatal neurons and Purkinje cells appeared coincidently. Our quantitative analysis has revealed that the number of labeled neurons was increased exponentially, first in the caudal motor-related areas, then in the rostral motor-related areas, and finally in the prefrontal areas (Bates and Goldman-Rakic, 1993; Luppino et al., 2003; Takada et al., 2004). In addition, the rapid increase in labeled neuron number could be ascribed to transneuronal labeling through intrinsic and/or bypath circuits. It should also be emphasized here that viral transport might not necessarily be restricted to the frontal

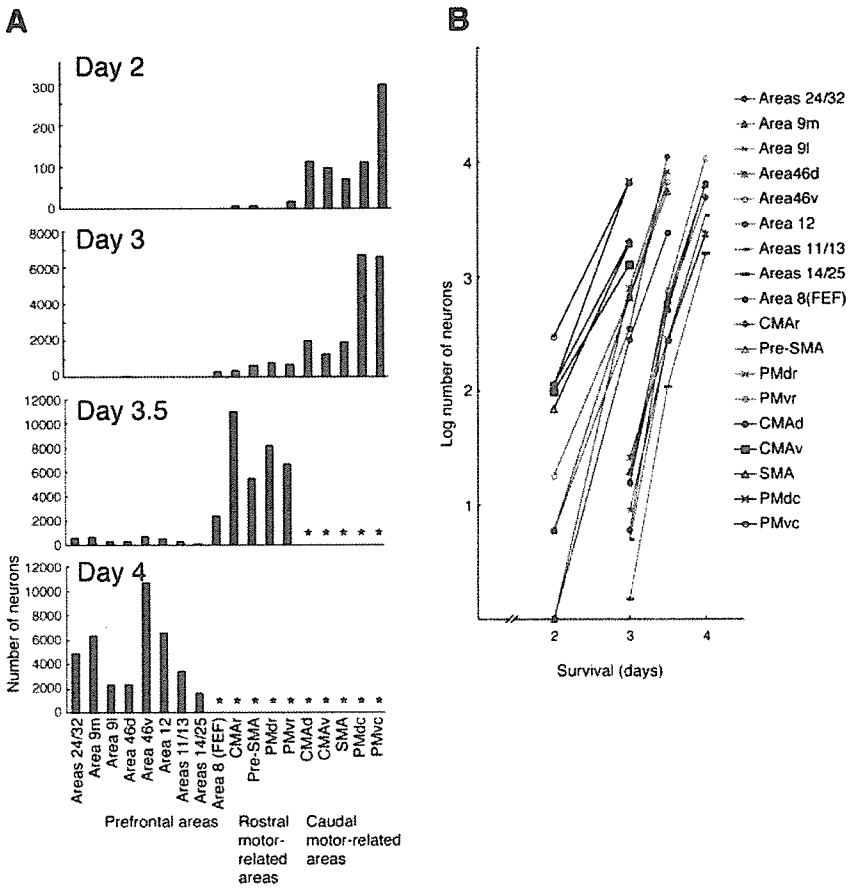

Figure 7. *A*, Diagrams showing the time-dependent changes in the number of labeled neurons in the frontal lobe. Cell counts were performed in every 12th section (60 μm thick; 720 μm apart). The cell number obtained at the 3, 3.5, or 4 d postinjection period is the average of data in monkeys Hu and Ke, Ir and Ta, or No and Ji, respectively, whereas the cell number at the 2 d postinjection period is taken from monkey Ma (see Table 1). Asterisks indicate the areas in which cell counts were not performed, because a tremendous number of neurons were labeled at the 3.5 and 4 d postinjection periods. *B*, Exponential increases in labeled neuron number with the postinjection period. The ordinate indicates the logarithm for the number of labeled neurons in each area. Black symbols represent the caudal motor-related areas, blue symbols represent the rostral motor-related areas, and red symbols represent the prefrontal areas. Filled purple circles represent area 8 (FEF). 9l, Lateral area 9; 9m, medial area 9; 46d, dorsal area 46; 46v, ventral area 46. Numbers correspond to the area numbers defined by Barbas and Pandya (1989).

lobe. The posterior parietal cortex, for instance, may mediate transport from the MI to the premotor and prefrontal areas (Cavada and Goldman-Rakic, 1989; Stanton et al., 1995). Labeling of prefrontal areas may be achieved via the ventral striatum–basal forebrain–MI link (Haber et al., 1990; Ferry et al., 2000).

The primary goals of the present study were (1) to elucidate whether or not the forelimb might specifically be represented in particular areas of the prefrontal cortex and (2) to explore whether or not the forelimb versus the hindlimb might differentially be represented in the prefrontal cortex.

The present results have demonstrated that ventral area 46 was most strongly labeled with rabies virus injected into forelimb representation of the MI. In contrast, dorsal area 46 exhibited much weaker labeling. This indicates that ventral area 46, but not dorsal area 46, is preferentially involved in the control of forelimb movements, albeit both areas are directly interconnected with the rostral motor-related areas (Arikuni et al., 1980; Barbas and Pandya, 1987; Lu et al., 1994; Takada et al., 2004). Consistent with our findings, previous physiological studies have reported that ventral area 46 neurons were specifically activated during the performance of delayed response tasks, in which monkeys responded manually (di Pellegrino and Wise, 1991; Hoshi et al., 1998; Rainer et al., 1998). On the other hand, both ventral and dorsal area 46 neurons responded to delayed oculomotor tasks (Funahashi et al., 1990, 1991). From an anatomical point of view, ventral area 46 and area 12 receive inputs mainly from the posterior parietal cortex (primarily area 7b) and the inferior temporal cortex, respectively (Barbas and Mesulam, 1985; Barbas, 1988; Cavada and Goldman-Rakic, 1989; Seltzer and Pandya, 1989; Carmichael and Price, 1995b). Moreover, it has been shown that posterior parietal neurons respond to forelimb movements as well as to somatosensory or visual stimuli (Dong et al., 1994; Calton et al., 2002).

The medial prefrontal cortex, including areas 24/32 and medial area 9, was another site of dense labeling from the MI forelimb region. Anatomical data to date indicate that these areas have direct interconnections with the rostral motor-related areas, such as the pre-SMA, CMAr, and PMdr (Barbas and Pandya, 1987; Luppino et al., 1993). Also, the medial prefrontal areas receive limbic (emotional or motivational) information from the amygdala and the parahippocampal cortex, as well as polymodal sensory information from the superior temporal cortex and the granular insular cortex (Barbas, 1988; Seltzer and Pandya, 1989; Barbas et al., 1999). Recently, physiological studies in humans and nonhuman primates have suggested that the medial prefrontal areas, including regions in the anterior cingulate cortex, participate in the selection of motor behaviors based on context or reward (Paus, 2001; Swick and Turken, 2002; Dreher and Grafman, 2003; Isomura et al., 2003; Matsumoto et al., 2003). Thus, the strong connectivity to the MI forelimb region implies that the medial prefrontal areas may be responsible for cognitive control of forelimb movements.

To address the issue on prefrontal representations of the forelimb versus the hindlimb, we compared the distribution patterns of prefrontal labeling from both regions of the MI. In the prefrontal cortex, much fewer neurons were labeled from the hindlimb than forelimb region. Ventral area 46, which had the densest labeling from forelimb representation, displayed only sparse labeling from hindlimb representation. Instead, the strongest labeling from hindlimb representation was located on the medial wall, especially in areas 24/32 and medial area 9. These findings imply that the medial prefrontal areas might closely be associated with the control of not only forelimb but also hindlimb movements.

In the present study, the viral injection into the MI forelimb region yielded labeling in prearcuate area 8, corresponding to the FEF. Substantial labeling of FEF neurons occurred as early as 3 d after the injection. This timing of transneuronal labeling coincides well with the timing for the rostral motor-related areas rather than the timing for the prefrontal areas. In the hindlimb-injection case, on the other hand, only a few neurons were labeled

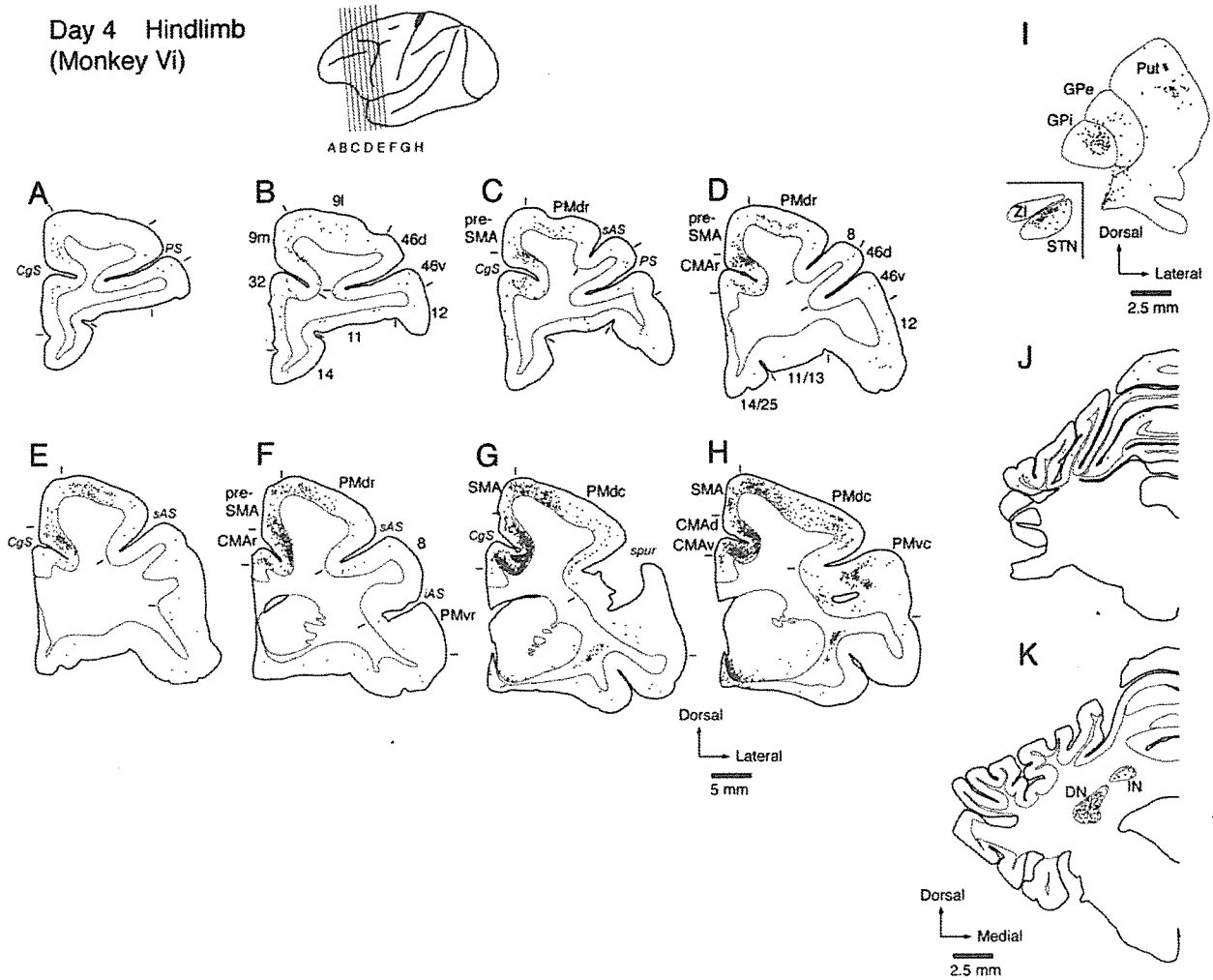

Figure 8. Distribution patterns of retrograde labeling in the frontal lobe (*A–H*), the basal ganglia (*I*), and the cerebellum (*J*, *K*) 4 d after the viral injection into the MI hindlimb region (monkey Vi). Eight representative coronal sections through the prefrontal cortex are arranged rostrocaudally in *A–H*. The approximate rostrocaudal levels of the sections are indicated in the lateral view of the brain. The dark area in this view specifies the extent of the injection site. In *I*, clusters of labeled neurons in the GPi, external segments of the globus pallidus (GPe), and the putamen (Put) are distributed more dorsally than those seen after the viral injection into the MI forelimb region (see Fig. 6*L*). As in the forelimb-injection case, another cluster of labeled neurons is located far ventromedially within the putamen (Kelly and Strick, 2004). In this case, the labeling of Purkinje cells occurs at the rostral level of the cerebellar cortex (*J*), and the labeled neurons in the cerebellar dentate nucleus (DN) and cerebellar interpositus nucleus (IN) are distributed more rostrally than in the forelimb-injection case (see Fig. 6*M*). Each dot in *A–K* corresponds to two labeled cells. CgS, Cingulate sulcus; iAS, inferior limb of the arcuate sulcus; PS, principal sulcus; sAS, superior limb of the arcuate sulcus; spur, spur of the arcuate sulcus; STN, subthalamic nucleus; ZI, zona incerta; 9l, lateral area 9; 9m, medial area 9; 46d, dorsal area 46; 46v, ventral area 46. Numbers correspond to the area numbers defined by Barbas and Pandya (1989).

in the FEF even on the fourth day. These data indicate that the FEF is strongly and specifically interconnected, via one synapse, with the MI forelimb region. This seems intriguing given that the FEF has rarely been implicated in the control of forelimb movements. Two pieces of evidence have addressed the issue on the possible involvement of the FEF in somatic motor control. Arikuni et al. (1988) have reported the existence of reciprocal connections between the FEF and the premotor cortex. Oishi and Kubota (1990) have shown that disinhibition of the FEF with the GABA antagonist bicuculline induces forelimb movements in behaving monkeys. Together, the present results suggest that the FEF is likely to play an essential role not only in the control of eye movements per se, but also in the control of eye–hand coordinative behaviors.

The present data define anatomical evidence for the differential patterns of distribution of prefrontal neurons that are multisynaptically connected with forelimb versus hindlimb representations of the MI. Our results favor a notion that cognitive behaviors based on prefrontal signals must be accompanied more frequently by actions manipulated with the forelimb than those with the hindlimb. Thus, the input systems from the prefrontal cortex to the MI might be developed in a use-dependent manner. Furthermore, the present results indicate that the medial prefrontal areas strongly innervate both the forelimb and the hindlimb regions of the MI in a multisynaptic manner. This suggests that movements of not only the forelimb but also the hindlimb could be influenced by signals derived from the prefrontal areas that receive limbic (amygdalar and hippocampal) inputs.

References

Arikuni T, Sakai M, Hamada I, Kubota K (1980) Topographical projections from the prefrontal cortex to the post-arcuate area in the rhesus monkey, studied by retrograde axonal transport of horseradish peroxidase. Neurosci Lett 19:155–160.

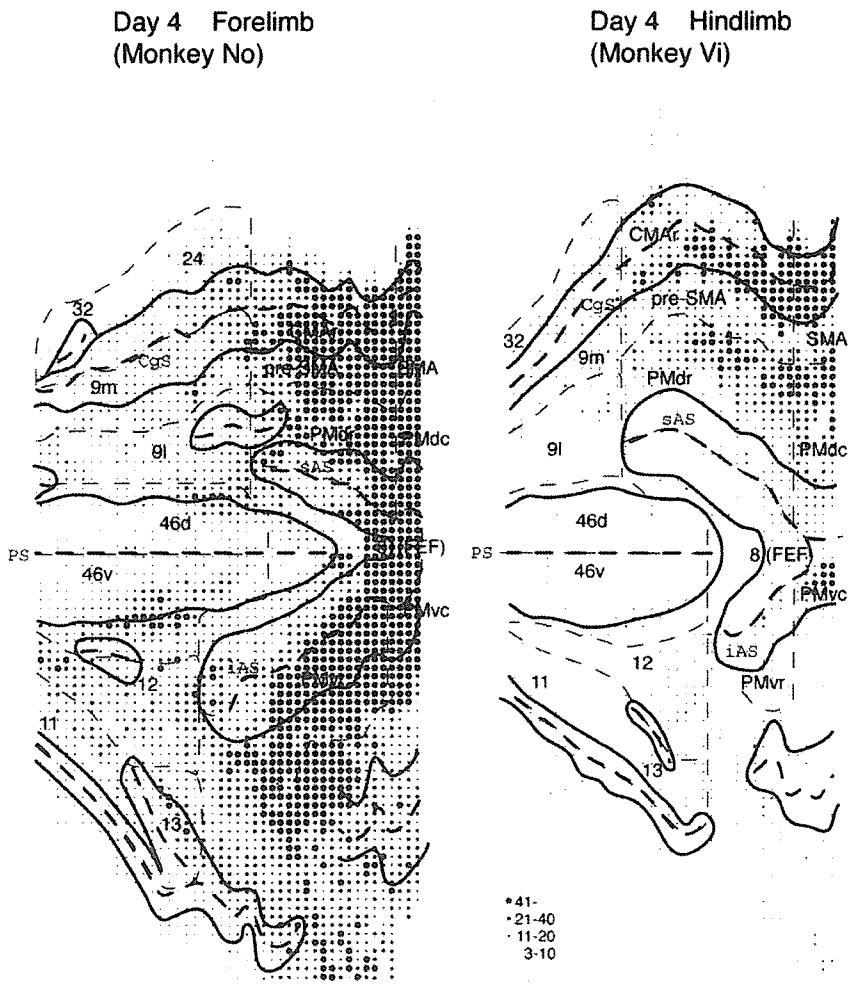

Figure 9. Surface-view reconstructions showing the distribution patterns of labeled neurons in the prefrontal cortex 4 d after the viral injections into the forelimb (monkey No) or hindlimb (monkey Vi) region of the MI. Black solid and dashed lines indicate the gyri and the fundi of the sulci, respectively. Thinner dashed lines denote the boundaries among the prefrontal areas. Four different sizes of filled circles represent the ranges of labeled neuron number. CgS, Cingulate sulcus; iAS, inferior limb of the arcuate sulcus; PS, principal sulcus; sAS, superior limb of the arcuate sulcus; 9l, lateral area 9; 9m, medial area 9; 46d, dorsal area 46; 46v, ventral area 46. Numbers correspond to the area numbers defined by Barbas and Pandya (1989).

Arikuni T, Watanabe K, Kubota K (1988) Connections of area 8 with area 6 in the brain of the macaque monkey. J Comp Neurol 277:21–40.

Barbas H (1988) Anatomic organization of basoventral and mediodorsal visual recipient prefrontal regions in the rhesus monkey. J Comp Neurol 276:313–342.

Barbas H, Mesulam MM (1985) Cortical afferent input to the principalis region of the rhesus monkey. Neuroscience 15:619–637.

Barbas H, Pandya DN (1987) Architecture and frontal cortical connections of the premotor cortex (area 6) in the rhesus monkey. J Comp Neurol 256:211–228.

Barbas H, Pandya DN (1989) Architecture and intrinsic connections of the prefrontal cortex in the rhesus monkey. J Comp Neurol 286:353–375.

Barbas H, Ghashghaei H, Dombrowski SM, Rempel-Clower NL (1999) Medial prefrontal cortices are unified by common connections with superior temporal cortices and distinguished by input from memory-related areas in the rhesus monkey. J Comp Neurol 410:343–367.

Bates JF, Goldman-Rakic PS (1993) Prefrontal connections of medial motor areas in the rhesus monkey. J Comp Neurol 336:211–228.

Calton JL, Dickinson AR, Snyder LH (2002) Non-spatial, motor-specific activation in posterior parietal cortex. Nat Neurosci 5:580–588.

Carmichael ST, Price JL (1995a) Limbic connections of the orbital and medial prefrontal cortex in macaque monkeys. J Comp Neurol 363:615–641.

Carmichael ST, Price JL (1995b) Sensory and premotor connections of the orbital and medial prefrontal cortex of macaque monkeys. J Comp Neurol 363:642–664.

Cavada C, Goldman-Rakic PS (1989) Posterior parietal cortex in rhesus monkey: II. Evidence for segregated corticocortical networks linking sensory and limbic areas with the frontal lobe. J Comp Neurol 287:422–445.

di Pellegrino G, Wise SP (1991) A neurophysiological comparison of three distinct regions of the primate frontal lobe. Brain 114:951–978.

Dong WK, Chudler EH, Sugiyama K, Roberts VJ, Hayashi T (1994) Somatosensory, multisensory, and task-related neurons in cortical area 7b (PF) of unanesthetized monkeys. J Neurophysiol 72:542–564.

Dreher JC, Grafman J (2003) Dissociating the roles of the rostral anterior cingulate and the lateral prefrontal cortices in performing two tasks simultaneously or successively. Cereb Cortex 13:329–339.

Dum RP, Strick PL (1991) The origin of corticospinal projections from the premotor areas in the frontal lobe. J Neurosci 11:667–689.

Dum RP, Strick PL (1996) Spinal cord terminations of the medial wall motor areas in macaque monkeys. J Neurosci 16:6513–6525.

Dum RP, Strick PL (2003) An unfolded map of the cerebellar dentate nucleus and its projections to the cerebral cortex. J Neurophysiol 89:634–639.

Ferry AT, Ongur D, An X, Price JL (2000) Prefrontal cortical projections to the striatum in macaque monkeys: evidence for an organization related to prefrontal networks. J Comp Neurol 425:447–470.

Flaherty AW, Graybiel AM (1993) Two input systems for body representations in the primate striatal matrix: experimental evidence in the squirrel monkey. J Neurosci 13:1120–1137.

Funahashi S, Bruce CJ, Goldman-Rakic PS (1990) Visuospatial coding in primate prefrontal neurons revealed by oculomotor paradigms. J Neurophysiol 63:814–831.

Funahashi S, Bruce CJ, Goldman-Rakic PS (1991) Neuronal activity related to saccadic eye movements in the monkey's dorsolateral prefrontal cortex. J Neurophysiol 65:1464–1483.

Galea MP, Darian-Smith I (1994) Multiple corticospinal neuron populations in the macaque monkey are specified by their unique cortical origins, spinal terminations, and connections. Cereb Cortex 4:166–194.

Georgopoulos AP, Kalaska JF, Caminiti R, Massey JT (1982) On the relations between the direction of two-dimensional arm movements and cell discharge in primate motor cortex. J Neurosci 2:1527–1537.

Haber SN, Lynd E, Klein C, Groenewegen HJ (1990) Topographic organization of the ventral striatal efferent projections in the rhesus monkey: an anterograde tracing study. J Comp Neurol 293:282–298.

Hatanaka N, Nambu A, Yamashita A, Takada M, Tokuno H (2001) Somatotopic arrangement and corticocortical inputs of the hindlimb region of the primary motor cortex in the macaque monkey. Neurosci Res 40:9–22.

He SQ, Dum RP, Strick PL (1993) Topographic organization of corticospinal projections from the frontal lobe: motor areas on the lateral surface of the hemisphere. J Neurosci 13:952–980.

Hikosaka K, Watanabe M (2000) Delay activity of orbital and lateral prefrontal neurons of the monkey varying with different rewards. Cereb Cortex 10:263–271.

Holsapple JW, Preston JB, Strick PL (1991) The origin of thalamic inputs to the "hand" representation in the primary motor cortex. J Neurosci 11:2644–2654.

Hoover JE, Strick PL (1999) The organization of cerebellar and basal ganglia outputs to primary motor cortex as revealed by retrograde transneuronal transport of herpes simplex virus type 1. J Neurosci 19:1446–1463.

Hoshi E, Shima K, Tanji J (1998) Task-dependent selectivity of movement-

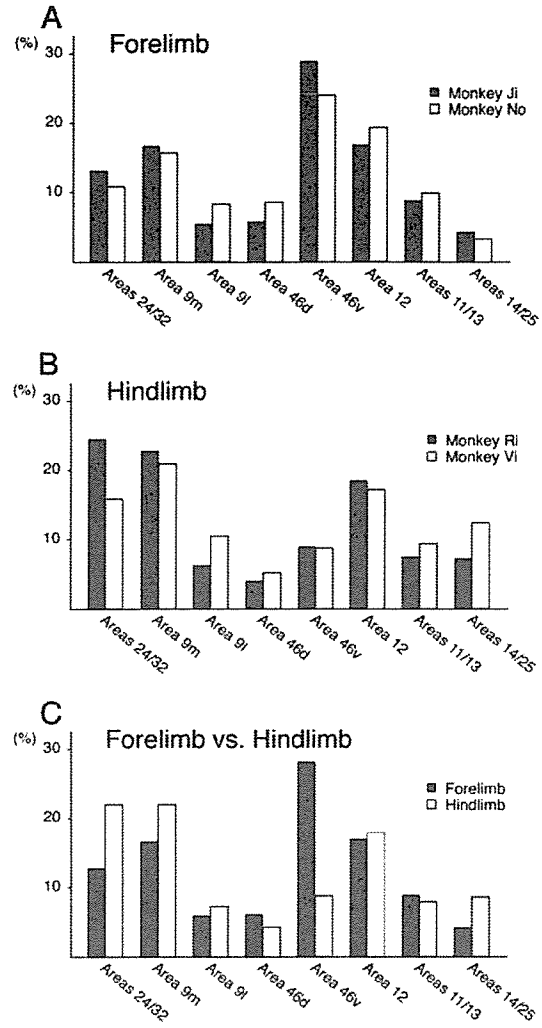

Figure 10. Diagram showing the differential distributions of neuronal labeling in the prefrontal cortex 4 d after the viral injections into the forelimb or hindlimb region of the MI (see also Fig. 9). *A*, *B*, Comparison of data obtained in two monkeys that received the injections into the forelimb region (*A*; monkeys Ji and No) or hindlimb region (*B*; monkeys Ri and Vi). Each bar represents the ratio of the labeled neuron number to the total number of labeled prefrontal neurons. Note that in each of the forelimb- and hindlimb-injection cases, the data are mostly consistent in the two monkeys. *C*, Comparison of the forelimb- versus hindlimb-injection cases. Filled and open bars indicate the average of the data obtained in the two monkeys shown in *A* and *B*, respectively.

related neuronal activity in the primate prefrontal cortex. J Neurophysiol 80:3392–3397.

Huerta MF, Krubitzer LA, Kaas JH (1987) Frontal eye field as defined by intracortical microstimulation in squirrel monkeys, owl monkeys, and macaque monkeys. II. Cortical connections. J Comp Neurol 265:332–361.

Inoue S, Sato Y, Hasegawa H, Noguchi A, Yamada A, Kurata T, Iwasaki T (2003) Cross-reactive antigenicity of nucleoproteins of lyssaviruses recognized by a monospecific anti-rabies virus nucleoprotein antiserum on paraffin sections of formalin-fixed tissues. Pathol Int 53:525–533.

Isomura Y, Ito Y, Akazawa T, Nambu A, Takada M (2003) Neural coding of "attention for action" and "response selection" in primate anterior cingulate cortex. J Neurosci 23:8002–8012.

Itoh K, Yasui Y, Takada M, Mitani A, Kaneko T, Sugimoto T, Mizuno N (1984) An anterograde-retrograde transneuronal transport of conjugates of wheat germ agglutinin with horseradish peroxidase (WGA-HRP): labeling of neurons in the reticular nucleus of the thalamus with WGA-HRP injected into the posterior column nuclei in the cat. Brain Res 323:185–187.

Kakei S, Hoffman DS, Strick PL (1999) Muscle and movement representations in the primary motor cortex. Science 285:2136–2139.

Kelly RM, Strick PL (2000) Rabies as a transneuronal tracer of circuits in the central nervous system. J Neurosci Methods 103:63–71.

Kelly RM, Strick PL (2003) Cerebellar loops with motor cortex and prefrontal cortex of a nonhuman primate. J Neurosci 23:8432–8444.

Kelly RM, Strick PL (2004) Macro-architecture of basal ganglia loops with the cerebral cortex: use of rabies virus to reveal multisynaptic circuits. Prog Brain Res 143:449–459.

Lu MT, Preston JB, Strick PL (1994) Interconnections between the prefrontal cortex and the premotor areas in the frontal lobe. J Comp Neurol 341:375–392.

Luppino G, Matelli M, Camarda R, Rizzolatti G (1993) Corticocortical connections of area F3 (SMA-proper) and area F6 (pre-SMA) in the macaque monkey. J Comp Neurol 338:114–140.

Luppino G, Rozzi S, Calzavara R, Matelli M (2003) Prefrontal and agranular cingulate projections to the dorsal premotor areas F2 and F7 in the macaque monkey. Eur J Neurosci 17:559–578.

Matsumoto K, Suzuki W, Tanaka K (2003) Neuronal correlates of goal-based motor selection in the prefrontal cortex. Science 301:229–232.

Muakkassa KF, Strick PL (1979) Frontal lobe inputs to primate motor cortex: evidence for four somatotopically organized "premotor" areas. Brain Res 177:176–182.

Oishi T, Kubota K (1990) Disinhibition in the monkey prefrontal cortex, by injecting bicuculline, induces forelimb movements learned in a GO/NO-GO task. Neurosci Res 8:202–209.

Pandya DN, Yeterian EH (1990) Prefrontal cortex in relation to other cortical areas in rhesus monkey: architecture and connections. Prog Brain Res 85:63–94.

Paus T (2001) Primate anterior cingulate cortex: where motor control, drive and cognition interface. Nat Rev Neurosci 2:417–424.

Rainer G, Asaad WF, Miller EK (1998) Memory fields of neurons in the primate prefrontal cortex. Proc Natl Acad Sci USA 95:15008–15013.

Sakagami M, Tsutsui K (1999) The hierarchical organization of decision making in the primate prefrontal cortex. Neurosci Res 34:79–89.

Seltzer B, Pandya DN (1989) Frontal lobe connections of the superior temporal sulcus in the rhesus monkey. J Comp Neurol 281:97–113.

Shindo K, Shima K, Tanji J (1995) Spatial distribution of thalamic projections to the supplementary motor area and the primary motor cortex: a retrograde multiple labeling study in the macaque monkey. J Comp Neurol 357:98–116.

Smith JS, Yager PA, Baer GM (1996) A rapid tissue culture test for determining rabies-neutralizing antibody. In: Laboratory techniques in rabies, Ed 4 (Meslin FX, Kaplan MM, Koprowski H, eds), pp 371–373. Geneva: World Health Organization.

Stanton GB, Bruce CJ, Goldberg ME (1995) Topography of projections to posterior cortical areas from the macaque frontal eye fields. J Comp Neurol 353:291–305.

Swick D, Turken AU (2002) Dissociation between conflict detection and error monitoring in the human anterior cingulate cortex. Proc Natl Acad Sci USA 99:16354–16359.

Takada M, Tokuno H, Nambu A, Inase M (1998) Corticostriatal projections from the somatic motor areas of the frontal cortex in the macaque monkey: segregation versus overlap of input zones from the primary motor cortex, the supplementary motor area, and the premotor cortex. Exp Brain Res 120:114–128.

Takada M, Nambu A, Hatanaka N, Tachibana Y, Miyachi S, Taira M, Inase M (2004) Organization of prefrontal outflow toward frontal motor-related areas in macaque monkeys. Eur J Neurosci 19:3328–3342.

Tokuno H, Tanji J (1993) Input organization of distal and proximal forelimb areas in the monkey primary motor cortex: a retrograde double labeling study. J Comp Neurol 333:199–209.

Tremblay L, Schultz W (1999) Relative reward preference in primate orbitofrontal cortex. Nature 398:704–708.

Ugolini G (1995) Specificity of rabies virus as a transneuronal tracer of motor networks: transfer from hypoglossal motoneurons to connected second-order and higher order central nervous system cell groups. J Comp Neurol 356:457–480.

Wilson FA, Scalaidhe SP, Goldman-Rakic PS (1993) Dissociation of object and spatial processing domains in primate prefrontal cortex. Science 260:1955–1958.